Chapter 4
Circulation

Dong-Kyu Lee, Young Ho Seung, Yun-Bae Kim, Young Ho Kim, Hong-Ryeol Shin, Chang-Woong Shin and Kyung-Il Chang

Abstract Recent basin-wide direct observations of near-surface circulation in the East Sea (Japan Sea), using satellite technology, reveal new circulation features. The East Korea Warm Current and Eastern Branch, originating from the Tsushima Warm Current, join to form the East Sea Current in the interior of the southern East Sea after leaving the coast. The formation mechanisms of the East Korea Warm Current and the Eastern Branch are diverse and their detailed dynamics are discussed in this chapter. The East Sea Current then exits the East Sea mainly through the Tsugaru Strait and this new current system is well reproduced by numerical models. The

D.-K. Lee (✉)
Department of Oceanography, Pusan National University, Busan 609-735, Republic of Korea
e-mail: dglee@pnu.edu

Y.H. Seung
Department of Oceanography, Inha University, Incheon 402-751, Republic of Korea
e-mail: seung@inha.ac.kr

Y.-B. Kim
Ulleungdo-Dokdo Ocean Science Station, Korea Institute of Ocean Science and Technology, Ulleung-Gun 799-823, Republic of Korea
e-mail: dokdo512@kiost.ac.kr

Y.H. Kim · C.-W. Shin
Physical Oceanography Division, Korea Institute of Ocean Science and Technology, Ansan 426-744, Republic of Korea
e-mail: yhkim@kiost.ac.kr

C.-W. Shin
e-mail: cwshin@kiost.ac.kr

H.-R. Shin
Department of Atmospheric Science, Kongju National University, Kongju 314-701, Republic of Korea
e-mail: hrshin@kongju.ac.kr

K.-I. Chang
School of Earth and Environmental Sciences, Seoul National University, Seoul 151-742, Republic of Korea
e-mail: kichang@snu.ac.kr

K.-I. Chang et al. (eds.), *Oceanography of the East Sea (Japan Sea)*,
DOI 10.1007/978-3-319-22720-7_4

Nearshore Branch and the North Korea Cold Current are only observed in summer months (May–August) and reversal of the North Korea Cold Current during winter is observed by the drifters. Mesoscale eddies are prevalent in the southern East Sea. They congregate in meridional bands and eddies are born, grow, propagate, and decay in a band determined by the vorticity of the mean flow. Many anticyclonic eddies in the Ulleung Basin (a negative vorticity zone) have life spans longer than one year, being sustained by kinetic energy received from the meandering mean flow. Deep water in the Japan Basin circulates cyclonically, and part of it penetrates into the southern Ulleung and Yamato basins through the channels and gaps. Deep cyclonic circulation in the Japan Basin appears to have strong mean currents of 4–8 cm s^{-1} along the perimeter of the basin and slow flows of 1–3 cm s^{-1} in the basin's interior. In the Ulleung Basin the deep flow is weak and highly variable with alternating cyclonic and anticyclonic sub-basin-scale cells. Deep circulation in the Japan Basin shows a distinct seasonal cycle with maximum speed in March and minimum speed in November. The seasonal variation of deep currents is not strong in the Ulleung and Yamato basins but the dominant variability is found to be in the 5–60-day period band. The deep circulation may be formed by cold-water convection rather than surface wind forcing, but the driving mechanism of the deep circulation is one of the unknown issues in the East Sea. Numerical simulations with realistic topography and forcing, high resolution, and lateral boundary conditions produce pictures of the circulation with many of the features observed in the entire East Sea, and they provide an opportunity to understand the dynamical processes of the East Sea circulation in detail. Numerical models with data assimilation have also been attempted successfully to interpret the near-surface and deep circulations in the East Sea.

Keywords Circulation · Currents · Dynamics · Numerical models · East Sea (Japan Sea)

4.1 Introduction

Maps of ocean near-surface circulation were historically drawn by compiling ship-drift data logged by sailors. Ship-drift data from merchant ships on the East Sea were scant and most of the information on the basin-scale surface circulation was based on hydrographic data. Uda (1934b) first performed basin-wide hydrographic surveys in the East Sea and was able to draw a current map which, until recently, was used extensively. Determination of the absolute current from hydrographic or Acoustic Doppler Current Profiler (ADCP) data has spatial and temporal limitations such as infrequent sampling, insufficient coverage by shipboard observation, and difficulty of defining a reference-level velocity in the shallow coastal sea. But basin-wide absolute current observations have been performed using recently developed satellite remote sensing technology. Sections 4.2 and 4.3 describe mean and temporal variations of East Sea near-surface circulation, including mesoscale eddies, based on 325 satellite-tracked drifters deployed mostly in 1996–2008, and satellite measurements of sea surface temperature (SST) and sea level anomaly (SLA).

The existence of the thermohaline circulation (THC) or the conveyor-belt system has often been referred to as one of the oceanic characteristics of the East Sea (Gamo 1999; Kim et al. 2001). As in the North Atlantic, the THC of the East Sea consists of deep-water formation processes (see Chap. 3 and references therein), interior upwelling processes, surface return flows (Park 2007), and deep circulation. The upwelling processes are largely unknown, however, mass balance considerations cast doubt on significant upwelling occurring across the 1800 m depth level in the central Ulleung Basin (UB) (Chang et al. 2009). Section 4.4 describes deep currents directly observed by Argo or Argo-type floats and current meter moorings in the East Sea as a branch of the THC, followed by a short review of the THC strength. Parking depths of the floats ranged from 700 to 800 m, but they are regarded as representing currents at 800 m since vertical current shear is weak. Water at 800 m depth corresponds to East Sea Central Water according to Kim et al. (2004a). The moored current measurements have been carried out mainly between 700 m depth and near the seabed. The history of float and moored current observations in the East Sea is introduced in Chap. 1. Water mass formation and characteristics of subsurface water masses with their variability are detailed in Chap. 3.

As described in Chap. 3, water masses in the East Sea are usually divided into three layers: the upper, intermediate, and deep layers. It is not clear whether circulation patterns also change from one water mass to another. Observations indicate that coupling between the upper layer occupied by Tsushima Warm Water (TWW) and the underlying layers is very weak, whereas that between the intermediate and deep layers is much stronger (Kim et al. 2009a). In fact, some observed deep currents show a weak bottom-trapped nature extending up to the intermediate layer, and are very different from the overlying currents carrying the TWW (Kim et al. 2013). Weak coupling between the upper and underlying layers can also be inferred dynamically from the fact that currents carrying the TWW are driven by inflow and outflow, whereas the underlying layers, nearly homogeneous in the vertical and much denser than the overlying layer, are isolated within the East Sea basin. The region north of the subpolar front, referred to as the cold-water region, is occupied by water colder than the TWW. In the cold-water region, the coupling between the upper layer and the underlying layers is not clear, but it seems to be stronger than that in the TWW region because of weaker stratification, especially in winter when the cold water-region loses much buoyancy through intense cooling (e.g. Seung and Yoon 1995a). Overall, the circulation in the East Sea may be divided largely into two regimes, the upper-layer circulation carrying the TWW and the underlying deep-layer circulation. It is noted, however, that the coupling between them, though weak, should be further quantified in future studies. Section 4.5 discusses some fundamental dynamical issues relating to upper- and deep-layer circulations in the East Sea, based on recent studies.

Early studies on dynamical processes in the East Sea employed numerical models with idealized and simple topography and coastline configurations. Although the simple models did not simulate realistic circulations and other phenomena in the East Sea, they have contributed to our understanding of the East Sea's circulation dynamics. With increasing computational resources since the 1990s, realistic configurations with real topography, time-varying meteorological forcing, and

improved open boundary conditions have appeared in modeling studies of the East Sea circulation. They have simulated realistic surface and sub-surface circulations, thereby expanding our understanding of the East Sea. Furthermore, sensitivity experiments of various numerical configurations have expanded our understanding of the relationship between small-scale phenomena and large-scale circulation in the East Sea. Numerical modeling has also advanced into an operational ocean forecast system. As ocean observational data have increased with advancing observing technology such as Argo floats, satellite remote sensing, and so on, ocean data assimilation techniques have been applied to numerical models in the East Sea. Section 4.6 describes numerical circulation models and data assimilated models which help us to understand observed circulation features of the East Sea.

4.2 Near-Surface Circulation

4.2.1 Mean Surface Current

Based on historical hydrographic data and current data from shipboard ADCPs, earlier studies (e.g. Katoh et al. 1996; Cho and Kim 2000) have suggested that the Tsushima Warm Current (TWC) entering into the East Sea splits into three currents: (1) The East Korea Warm Current (EKWC) flows along the eastern coast of Korea and enters the UB. (2) The Nearshore Branch follows the northern coast of Japan all the way up to the Tsugaru Strait. (3) The Offshore Branch flows into the Yamato Basin (YB) but its path is not as well defined as the other two branches. However, recent deployments of satellite-tracked drifters have revealed different mean flow patterns in the East Sea after the TWC passes through the Korea Strait (Lee and Niiler 2010a). More than 50 % of the time, drifters passing through the western channel of the Korea Strait followed the EKWC path along the Korean coast. The EKWC meanders after entering the UB and organizes itself into a broad East Sea Current after merging with the flow from the eastern channel of the Korea Strait (Eastern Branch) (Fig. 4.1; Lee and Niiler 2005). The EKWC behaves like Arruda et al.'s (2004) simple model in which eddies are generated by a meandering current and the mean current exits through the Tsugaru Strait. Most of the time, the current in the eastern channel of the Korea Strait (Eastern Branch in Fig. 4.1) flows along the coast of Japan either up to the Oki Bank or to the Noto Peninsula and then joins the East Sea Current (Fig. 4.1). In summer only, the Nearshore Branch of the TWC develops along the coast of Japan. The East Sea Current (Lee and Niiler 2005) is the broad current that the EKWC and Eastern Branch form after leaving the respective coasts of Korea and Japan. The naming of this new current is needed to address the observed features: that the EKWC becomes a strong mean current in the middle of the southern East Sea and that the Eastern Branch, most of the time, enters the YB after leaving the coast of Japan. This broad mean current system has also been reproduced well by recent high resolution numerical models (Luneva and Clayson 2006; Clayson et al. 2008).

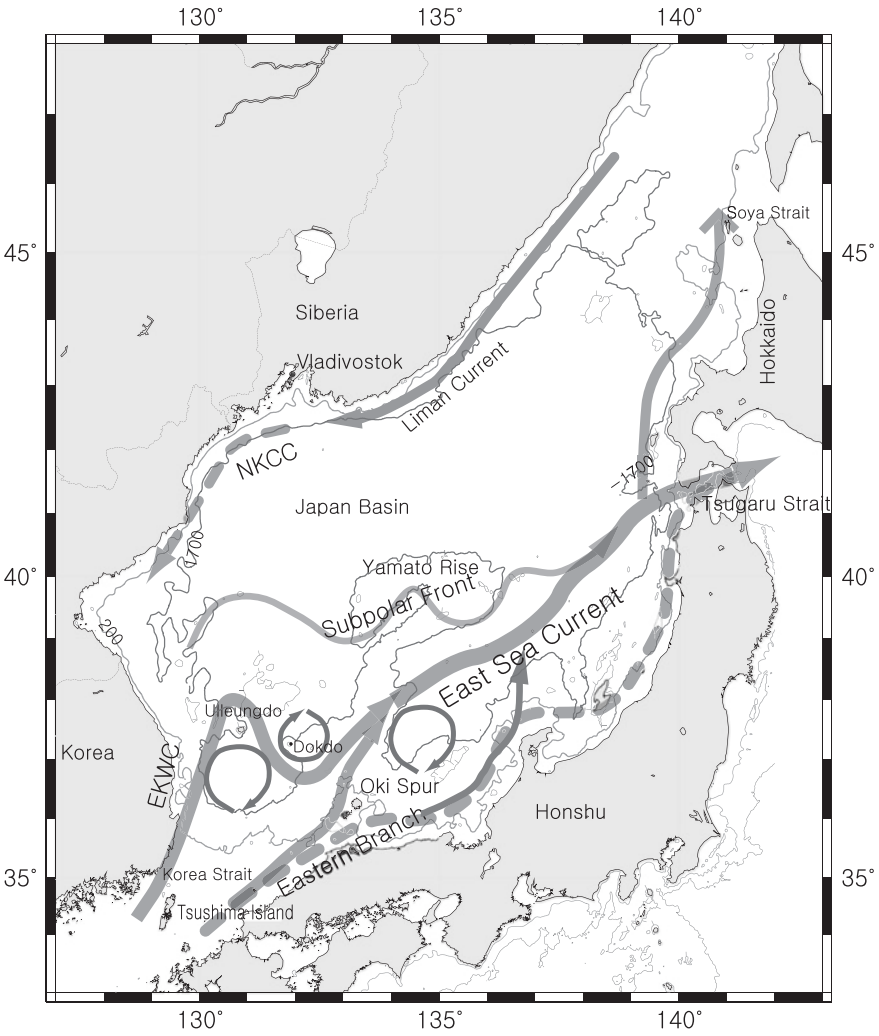

Fig. 4.1 Schematics of the surface circulation of the East Sea based on satellite tracked drifters. *Dotted lines* represent the current observed only in summer months (May–August)

More detailed descriptions of the southern East Sea surface circulation, including an historical view of the branching of the TWC, are found in Sect. 4.5.2.

In the northern East Sea, no distinctive year round mean current is observed except the Liman Current which flows southward along the Siberian coast down to Vladivostok (Fig. 4.1). The Liman Current, first described by Uda (1934a), derives from the freshwater flux related to ice melting in the Tatarsky Strait and from the wind drift (Martin and Kawase 1998; Park et al. 2006). Although the North Korea Cold Current (NKCC) appears, from numerical model simulation, throughout the seasons with seasonal transport variation (Kim and Min 2008), it is only during

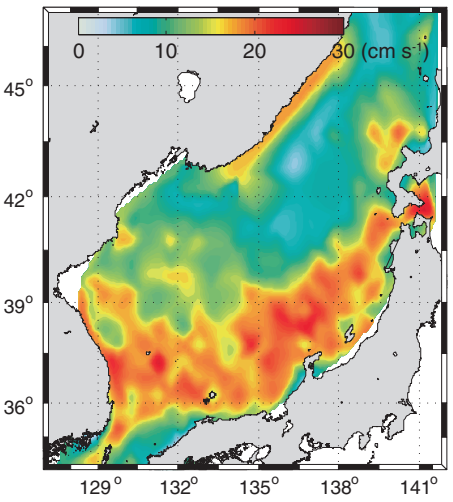

Fig. 4.2 Square root of eddy kinetic energy at the sea surface from surface drifter data (Redrawn from Lee and Niiler 2005)

summer that it has been observed from drifters. From over 325 drifters that were mostly deployed in the southern East Sea, only a few crossed the subpolar front between the warm-energetic southern East Sea and the cold-less-energetic northern East Sea (Fig. 4.2), and thus there were not many drifter observations in the northern East Sea from which a mean circulation can be defined.

4.2.2 Variability of the Surface Current and the Subpolar Front

The subpolar front divides the East Sea into two regions: (1) the energetic southern East Sea with large eddy kinetic energy (EKE) in which a strong mean flow enters the basin and exits through the Tsugaru and Soya straits, and (2) the calm northern East Sea with small EKE in which no distinctive year-round mean flow is found (Fig. 4.2). Historically the NKCC has been regarded as a year round mean current along the coast of North Korea (e.g. Kim and Min 2008). But large seasonal changes including a reversal of the NKCC have been observed (Yang 1996; Lee and Niiler 2005; Yoon et al. 2005). The subpolar front is observed year round nearly along 40°N in the northeastern East Sea (Fig. 4.1), but a separate front with characteristics similar to the subpolar front is found in the middle of the southern East Sea, formed by the reduced transport of warm water through the Korea Strait in spring (Lee and Niiler 2005). The subpolar front inferred from analyzing Lagrangian observations of individual float tracks may differ from the subpolar front described in Chap. 3, but it represents well the boundary between the less energetic northern East Sea and the energetic southern East Sea, formed by warm water inflow from the East China Sea through the Korea Strait.

The EKWC, after leaving the coast, forms various circulation patterns in the UB, depending on eddies and separation location from the coast (Katoh et al. 1996; Mitchell et al. 2005b). Three patterns from drifter tracks are recognized for the flow entering the East Sea through the western channel of the Korea Strait (Lee and Niiler 2010a): (1) Flow with large negative vorticity gains more negative vorticity from the deepening topography and so turns clockwise. It then joins the flow from the eastern channel of the Korea Strait and flows along the coast of Japan up to the Oki Spur (Tsushima Warm Current Pattern). (2) When the flow has mean speed over 55 cm s^{-1} with large positive vorticity, potential vorticity conservation applies and the EKWC follows the isobaths first along the coast and then along a topographic feature north of Ulleungdo (Ulleung Island) (Inertial Boundary Current Pattern). After entering the northern UB, the flow becomes an inertial meandering jet similar to a western boundary current. (3) The EKWC with small negative vorticity follows the southeastern coast of Korea up to 38°N (Ulleung Eddy Pattern) and meanders through the UB after entering it. Branching of the flow after passing through the western channel of the Korea Strait is found to occur only 15 % of the time; thus splitting or branching of the TWC at the entrance of the East Sea reported in hydrographic surveys and in theoretical studies is possibly attributable to the fact that the flow in each channel of the Korea Strait chooses a separate path.

Contrary to previous studies, the Nearshore Branch along the Japan coast and the NKCC along the North Korea coast are observed only in summer months (Lee and Niiler 2005). A northward NKCC along the coast up to the area west of Vladivostok in winter months is a surprising new observation. This reversal of the NKCC was observed from drifters (Yang 1996) and it has also shown up in a numerical model (Yoon et al. 2005). The Liman Current is assumed to be a year round current, but those far northern areas are too remote to aquire enough measurements for studying surface circulation.

4.2.3 Coastal Upwelling

The TWW along the east coast of Korea is carried by the northward flowing EKWC south of the subpolar front of the East Sea. The North Korea Cold Water (NKCW), originating from the western Japan Basin (JB) and carried by the NKCC, occupies the lower layer below the TWW with the permanent thermocline between them. In summer (June–August), the TWW includes the Low Salinity Tsushima Warm Water and High Salinity Tsushima Warm Water (HSTWW) (see Chap. 3), and the water column exhibits a three-layer structure. Due to the northward flowing EKWC and southward flowing NKCC underneath the EKWC (Byun and Seung 1984; Chang et al. 2002), isopycnals (isotherms) slope upward towards the coast. Subsurface isotherms further shoal and outcrop at the sea surface in summer when southerly winds prevail, and the surfacing of subsurface isotherms can occur in a few days (Byun 1989). Hence, coastal upwelling in the east coast

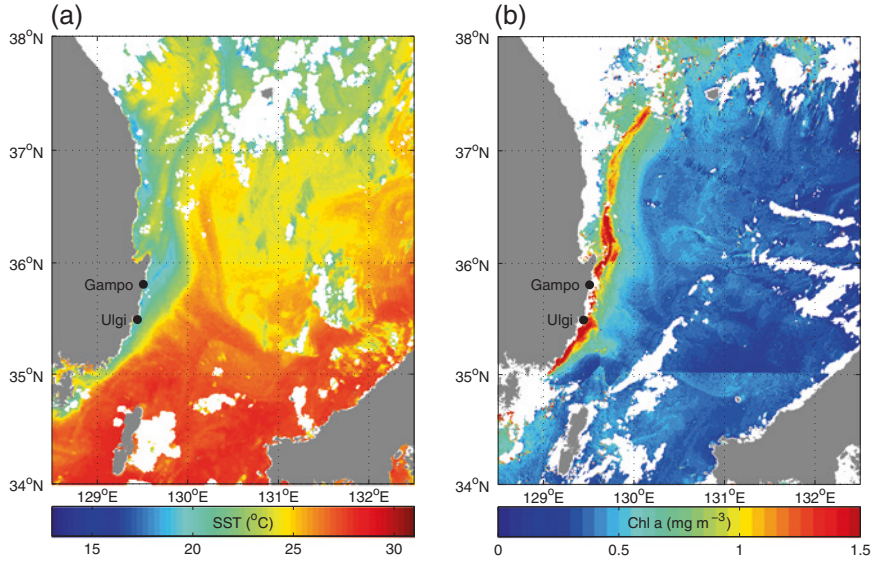

Fig. 4.3 Satellite images of **a** sea surface temperature from NOAA on 20 July 2013 and **b** chlorophyll *a* on 21 July 2013. Surface cold waters along the east coast of Korea including the Gampo-Ulgi area due to coastal upwelling can be seen. Coastal high chlorophyll water off Gampo-Ulgi area can also be seen together with offshore advection of cold and high-chlorophyll coastal water due to the East Korea Warm Current

of Korea occurs due to the combined effects of the background current (EKWC) and upwelling-favorable southerly winds (An 1974; Seung 1974; Lee 1983; Byun and Seung 1984; Lee and Na 1985). The source of cold waters upwelled to the sea surface can be either the HSTWW or the NKCW depending on the intensity of the upwelling (Kim and Kim 1983; Lee and Na 1985; Byun 1989; Lee et al. 1998).

The summertime southerly wind has been shown to be correlated with SST (Lee 1983; Lee et al. 2003b). Surface cold waters, however, have been frequently observed in a localized region, the Gampo-Ulgi area (GU area) (Fig. 4.3), although the southerly wind prevails along the entire east coast of Korea in summer. In the GU area, 80 % of southerly wind events caused the SST to drop more than 1.0 °C (Lee et al. 1998), and the SST decrease resulting from an upwelling-favorable wind occurs in 3–18 h (Lee et al. 2003b). Other factors responsible for localized upwelling in the GU area include steeply sloping isopycnals towards the coast due to an approach of the EKWC, local diverging topography, separation of the EKWC near Gampo, and the degree of stratification (Byun and Seung 1984; Lee and Na 1985; Lee et al. 1998, 2003b). Mean SST drops in the GU area during summer upwelling events are about 3.0–4.0 °C (Lee 1983; Lee et al. 1998) with a maximum SST drop of 12.2 °C in 1978 (Lee 1983) and an even bigger drop of 14.0 °C in 1997 at Gampo (Lee et al. 2003b). When strong winds (3–6 m s^{-1}) persisted for at least 3 days, upwelling events occurred, and the events persisted

for 3–33 days (Lee 1983). Byun (1989) applied a 3-layer model of upwelling (Csanady 1982) and showed that wind impulse, the time-integrated wind stress, during upwelling events in 1982 and 1983 ranged from 10 to 40 $m^2\ s^{-1}$, which corresponds to a wind blowing for 5–20 days with speed of 4 $m\ s^{-1}$.

In eastern boundary upwelling regions, significant correlations are often found between an upwelling-favorable wind and other variables than SST, such as coastal sea level and alongshore current (e.g. Smith 1974). On the other hand, coastal sea level is poorly correlated with wind in the GU area (Lee et al. 2003b) indicating other factors affecting the subtidal sea level variability (e.g. Lyu et al. 2002; Cho et al. 2014). Subtidal current fluctuations representing EKWC variation were also shown to be only marginally correlated with local wind (Lee et al. 2003b). Coastal upwelling in the GU area also occurred in spring (Byun and Seung 1984; Hyun et al. 2009).

The GU upwelling area often forms a semi-circle of cold water, with a radius of about 10–20 km from the coast to the upwelling front (Byun 1989). Satellite-derived SST images also showed that upwelled cold water in the GU area protrudes to the northeast (Byun 1989; Lee et al. 1998).

Seung (1984), using a simple 2-layer numerical model, suggested several possible upwelling centers, other than the GU area, along the east coast of Korea, due to coastal geometry. The satellite image in Fig. 4.3 clearly shows that coastal cold waters due to upwelling are also found in other coastal areas, which has been poorly documented. A report was given of an observation of the appearance of unusually cold surface water in the mid-east coast of Korea, north of the GU area, caused by the most intense southerly winds for the past 10 years resulting from a large-scale atmospheric condition (Park and Kim 2010).

Coastal upwelling at the east coast of Korea has important local and basin-scale consequences in terms of biogeochemical aspects (see Chap. 10). Locally, the GU upwelling area in summer is characterized by high primary production (Han et al. 1998), high chlorophyll fluorescene (Lee and Kim 2003), high zooplankton abundance (Lee et al. 2004), relatively low detritus percentage, high values of vertically integrated planktonic carbon, high percentage of particulate organic carbon and nitrogen in total suspended matter, and low ratio of particulate organic carbon to chlorophyll *a* (Yang et al. 1998) compared to those in offshore regions and in other seasons. The upwelled water in the area also has high dissolved oxygen content, low pH, and high alkalinity (Lee and Kim 2003). The oxygen rich upwelled water observed in 2001 suggests its origin from the NKCW rather than either the Japan Sea Proper Water or the TWW, at least in 2001 (Lee and Kim 2003).

Coastal waters with high productivity due to coastal upwelling are drawn offshore by large-scale circulation set by the EKWC and/or the mesosale circulation of the Ulleung Warm Eddy (UWE), resulting in enhanced biological productivity in the UB (Onitsuka et al. 2007; Hyun et al. 2009; Yoo and Park 2009) (Fig. 4.3). Without the coastal upwelling, the nutrient-depleted EKWC acted to decrease chlorophyll concentration in the middle of the UB (Son et al. 2014). Hence, the coastal upwelling together with surface circulation would be an important factor in

making the UB the most productive basin among the three basins of the East Sea (Yamada et al. 2005; Kwak et al. 2013).

Consecutive hydrographic data support the highly-variable nature of the coastal upwelling (Byun 1989; Lee and Kim 2003). On the other hand, time series data to reveal the multiple scale variability is scarce, partly due to heavy fishing activities in the coastal areas. More observational efforts are required to delineate the spatial and temporal structure of the upwelling and to unravel the physics behind the coastal upwelling. Also biogeochemical and ecosystem responses to coastal upwelling have not yet been fully addressed, although many studies have pointed out the importance of the coastal upwelling in maintaining high primary productivity in the UB. Even a qualitative description of coastal upwelling in coastal regions along the east coast of Korea other than the GU area is lacking.

4.3 Mesoscale Eddies

4.3.1 Characteristics of Eddies

The East Sea is one of the most eddy-rich regions of the world ocean (Ichiye and Takano 1988). In particular, many warm and cold eddies are found near the UB (Lie et al. 1995; Lee and Niiler 2005), and eddies in this region can be classified into three groups (Lee and Niiler 2010b): (1) coastal eddies along the Korean coast, (2) frontal eddies along meanders of the inertial boundary current, (3) UWE and Dok Cold Eddy (DCE). The UWE and DCE are clustered mostly in the negative and positive relative vorticity areas, respectively (Fig. 4.4). The UWE has the largest size (126 × 194 km) and longest mean life (171 days). Although the mean propagation direction of the UWE is southeastward, it sometimes moves northward along the Korean coast due to an oscillating EKWC (or subpolar front) meander and leaves the UB to enter the northern East Sea (Shin et al. 2005). The UWE originates from the EKWC and forms from a southward flow related to anticyclonic circulation around Ulleungdo (Tanioka 1968; Mitchell et al. 2005b). Arruda et al. (2004) argued that the UWE may not be related to instabilities but instead may be due to the effects of the meridional gradient of planetary vorticity (β) and nonlinearities. Temporal evolution of the UWE is presented in Sect. 4.3.2. When the EKWC is weak and linear, there is no eddy formation, in agreement with this observation.

The DCE is located south of Dokdo throughout much of the year (Fig. 4.5). The DCE is generated through an instability process, followed by a retreat of the subpolar front, when a large-amplitude meander pinches off between Ulleungdo and Dokdo (Mitchell et al. 2005a). The DCE is typically about 60 km in diameter and its center was observed between 130.5°E and 132°E from June 1999 to July 2001. After formation from the subpolar front, the DCE stays southwest of Dokdo for 1–6 months before propagating westward toward Korea where it merges with the EKWC, or is engulfed in a southward meander of the subpolar front. When the

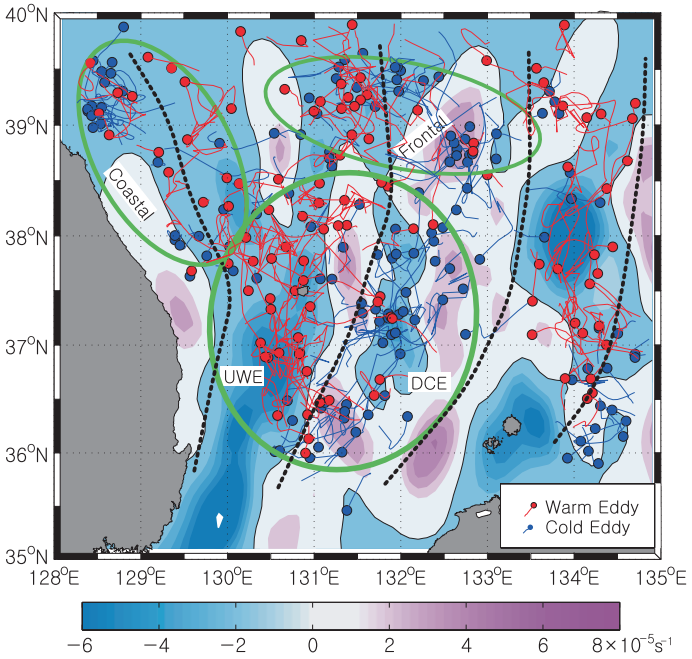

Fig. 4.4 Distribution and propagation of eddies plotted on a colored background of mean relative vorticity (*see color bar*). Four meridional bands of mean relative vorticity and three groups of eddies are demarcated by *dotted lines* and *green lines*, respectively (from Lee and Niiler 2010b)

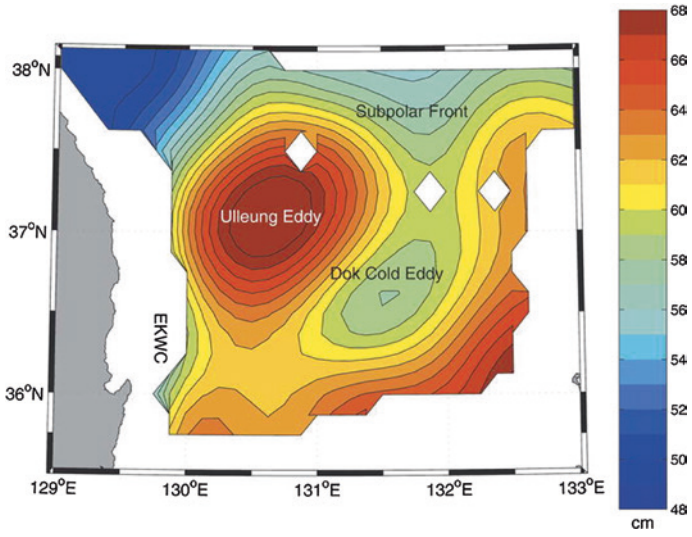

Fig. 4.5 Average dynamic height over a 2-yr deployment in the Ulleung Basin. The mean positions of the EKWC, Ulleung (Warm) Eddy, Subpolar Front, and the Dok Cold Eddy are labeled. The *white diamonds*, from *left* to *right*, are Ulleungdo (Ulleung Island), Dokdo (Dok Island), and a seamount that reaches within 500 m of the surface (from Mitchell et al. 2005a)

DCE approaches the Korean coast, the EKWC diverts eastward around it, suggesting that DCEs play an important role in the path of the EKWC.

Two to four warm eddies always exist in the YB (Isoda 1994; Morimoto et al. 2000) (Fig. 4.6). Warm eddies are generated in spring around the Oki Islands due to the flow over the bottom topography around the Oki Bank. After separating from the Oki Bank, the warm eddies move eastward along the Japanese coast or offshore from the Japanese coast. While they are moving, the warm eddies sometimes coalesce with neighboring warm eddies or split into multiple eddies. The warm eddies move continuously eastward from the Noto Peninsula in winter-spring with mean speeds of 0.5–2 cm s^{-1}, reaching the northwestern coast of Japan in the following winter. In there they typically split into two or three small eddies, and decay within a few months.

The presence of mesoscale eddies and their migration in the upper layer results not only in strong upper layer currents with associated low-frequency variability at a fixed location (Kim et al. 2009a) but also deep current fluctuations below 1000 m (Takematsu et al. 1999b) and excitation of topographic Rossby waves (Kim et al. 2013). Anticyclonic mesoscale eddies, like the UWE in the East Sea, also interact with near-inertial waves funneling near-inertial motions to the deep layer below the eddies (Park and Watts 2005) and reflecting near-inertial waves within the thermostad of the eddy (Byun et al. 2010) (see Chap. 5.4).

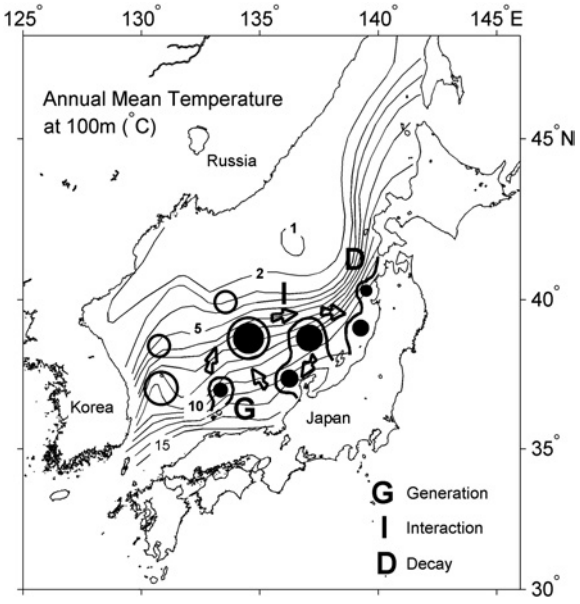

Fig. 4.6 Schematic illustration of the movement process of warm eddies in the southeastern East Sea. *Thin contour lines* indicate the horizontal distribution of annual mean temperature at 100 m depth (Redrawn from Isoda 1994)

4.3.2 Evolution of the Ulleung Warm Eddy

The horizontal distribution of temperature and salinity at a depth of 200 m is well suited for identifying warm eddies in the southwestern East Sea (Shin et al. 2005). In April 1993 the UWE (WE92) had a size of approximately 150 km east-west and 170 km north-south at 200-m depth (Fig. 4.7). The surface homogeneous layer of 10 °C (Ten Degrees Water, see Sect. 3.3.1) and 34.2 psu inside the UWE was produced by vertical convection from sea-surface cooling in winter, and deepened to a maximum of about 250 m in early spring. The homogeneous water displays positive oxygen and negative salinity anomalies relative to the surrounding thermocline water, indicative of formation from winter mixed layer water (Gordon et al. 2002). The deep homogeneous layer is a characteristic of a warm eddy that winters in the East Sea (Shin et al. 1995) and in the Kuroshio Extension (Tomosada 1986; Yasuda et al. 1992). From April to September, WE92 shrunk about 20 km in the east-west and about 80 km in the north-south directions (Fig. 4.7). The thickness of the homogeneous layer was also reduced to depths between 70 and 150 m. When the EKWC and the warm eddy converged around Ulleungdo, the EKWC

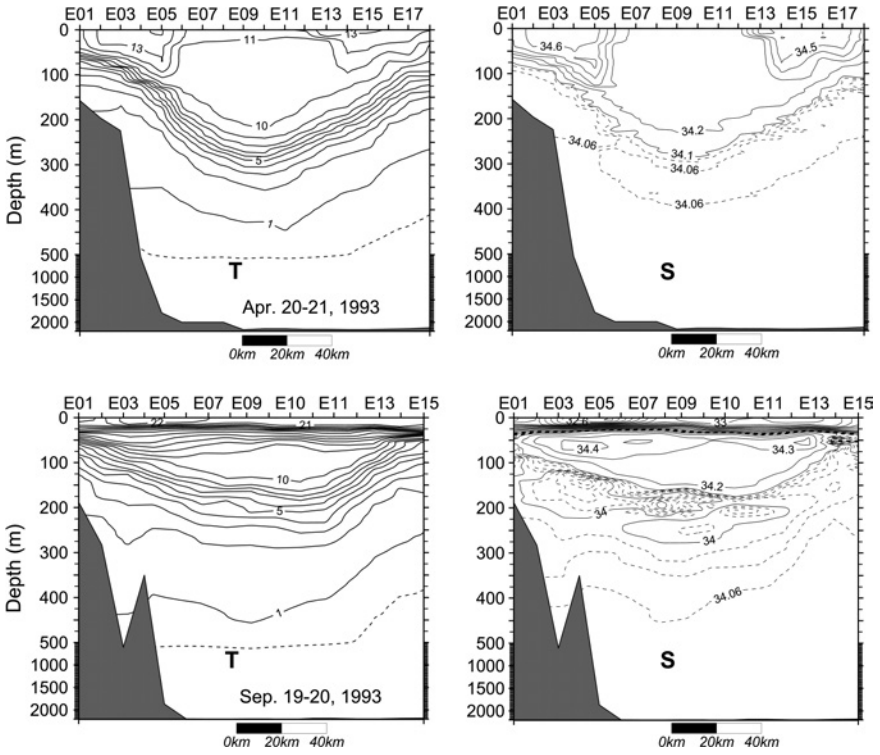

Fig. 4.7 Temperature (°C) and salinity (psu) vertical cross-sections in (*upper*) April and (*lower*) September 1993 (Redrawn from Shin et al. 2005)

supplied water of high temperature and salinity to the UWE; the EKWC flowed around the edge of the UWE in spring (Fig. 4.7) and gradually expanded into the inner portion during summer and fall.

Eddies are important to biological productivity, because of their association with upwelling of subsurface water. One of the mechanisms responsible for nutrient input into the euphotic zone is uplifting of the nutricline by cyclonic eddies, known as "eddy pumping," which results in enhanced primary production inside a cyclonic eddy (Falkowski et al. 1991). High primary productivity in the East Sea during late spring and early fall appears to be sustained by the interaction between eddies and wind, as well as other factors such as coastal upwelling and terrestrial nutrient input during the rainy season (e.g. Hyun et al. 2009).

4.4 Thermohaline Circulation

4.4.1 Rates of Water Mass Formation

The strength of the ocean's THC is often represented by a zonally integrated meridional streamfunction (MOC, meridional overturning circulation). The MOC can be calculated from full-depth hydrographic observations along latitude lines (Talley et al. 2003), numerical model results (Balmaseda et al. 2007), and direct observations (McCarthy et al. 2012). In the East Sea, it is difficult to calculate the MOC using hydrographic data, because the properties of thick deep water masses are almost homogeneous with little spatial density contrast. According to the meridional streamfunction based on numerical model results driven by climatological forcing, there exists a closed streamfunction similar to the Atlantic MOC although the East Sea's inflow-outflow system complicates the upper streamfunction field (Yoshikawa et al. 1999). Model-derived maximum East Sea MOC transport is about 0.6 Sv (1 Sv $= 10^6$ m^3 s^{-1}), and below 1500 m the maximum value is about 0.15 Sv.

The water mass formation rate may set the strength of the THC (Kuhlbrodt et al. 2007). The formation rate of the Upper Portion of the Japan Sea Proper Water (UPJSPW) lying in the 400–1000 m depth range was estimated to be 0.48 and 0.38 Sv, respectively, based on hydrographic data (Senjyu and Sudo 1996) and numerical model results forced by climatological forcing (Kawamura et al. 2007). Box models constrained by observed chemical tracers yielded two different total formation rates of subsurface water masses below 600 m prior to the 1960s: 0.65 Sv (Postlethwaite et al. 2005) and 1.41 Sv (Jenkins 2008). After the 1960s, both estimates decreased to 0.27 Sv, which is about a 60–80 % reduction of the formation rate for those water masses; this was ascribed to the slow-down of the East Sea THC (Gamo 1999). A study using a moving boundary box model (MBBM) also suggests a decline in Bottom Water formation in 2000 compared with that in 1960 (Kang et al. 2003). However, the total formation rate of East Sea Central, Deep, and Bottom Waters in 2000, 0.49 Sv, remained the same as

that in 1960 in the MBBM, suggesting a change from bottom water formation to upper water formation without any significant reduction of the total formation rate of sub-surface water masses.

4.4.2 Deep Currents and Circulation

One distinctive characteristic of the East Sea is the prevalence of spatially homogeneous deep waters below the pycnocline. Density-based dynamic calculation is thus impractical and would give misleading values for the deep currents. Studies of subsurface circulation of the East Sea have benefited from tracer distributions, numerical modeling, moored current measurements since the late 1980s, and deployments of floats since 1995. Compilations of data from the floats and moored current measurements allow construction of mean circulation maps for the entire East Sea (Senjyu et al. 2005; Choi and Yoon 2010; Park and Kim 2013). Two-year long continuous moored current and bottom pressure measurements between 1999 and 2001 revealed details of the UB deep circulation (Teague et al. 2005). Schematic circulation maps suggested by previous studies are shown in Fig. 4.8.

The subsurface currents below the pycnocline are characterized by weak vertical shear and barotropic fluctuations (Takematsu et al. 1999a; Senjyu et al. 2005; Chang et al. 2009). A limited number of full-depth current measurements from about 40 m to near the seabed shows that while low-passed subsurface current fluctuations below the pycnocline are coherent, the fluctuations of upper currents above 200 m are poorly correlated with those below the pycnocline (Kim et al. 2009a, 2013).

4.4.2.1 Mean Currents

Figure 4.9 shows bin-averaged mean currents at 800 m, together with EKE, with bin size of 0.5° in both longitude and latitude based on a compilation of float data from 1999 to 2010 (Park and Kim 2013). Also Fig. 4.10 shows mean currents at 82 locations measured at the deepest depth level of each mooring (below 1000 m except at 4 locations: U1, U6, Y16, Y17) by current meter moorings between 1986 and 2007. The mooring periods mostly exceed 6 months except at 7 locations (U1, U6, U14, from YB15 to YB18). The deep current map shown in Fig. 4.10 has been updated from previous studies (Chang et al. 2002; Senjyu et al. 2005; Teague et al. 2005) by adding more data available from various sources (MSA Reports 1995–2007; Jang 2011; Baek et al. 2014; Lee and Chang 2014). The eddy/mean kinetic energy ratio is superimposed on the mean current vectors at 800 m in Fig. 4.9b, and denoted by colored circles at mooring locations in the UB in Fig. 4.10b.

The mean features of the deep circulation are a basin-scale cyclonic circulation in each of the three deep basins (Fig. 4.8a), with strong currents along the basins' peripheries and weaker flows in the basins' interiors (Figs. 4.9a, 4.10). Strong

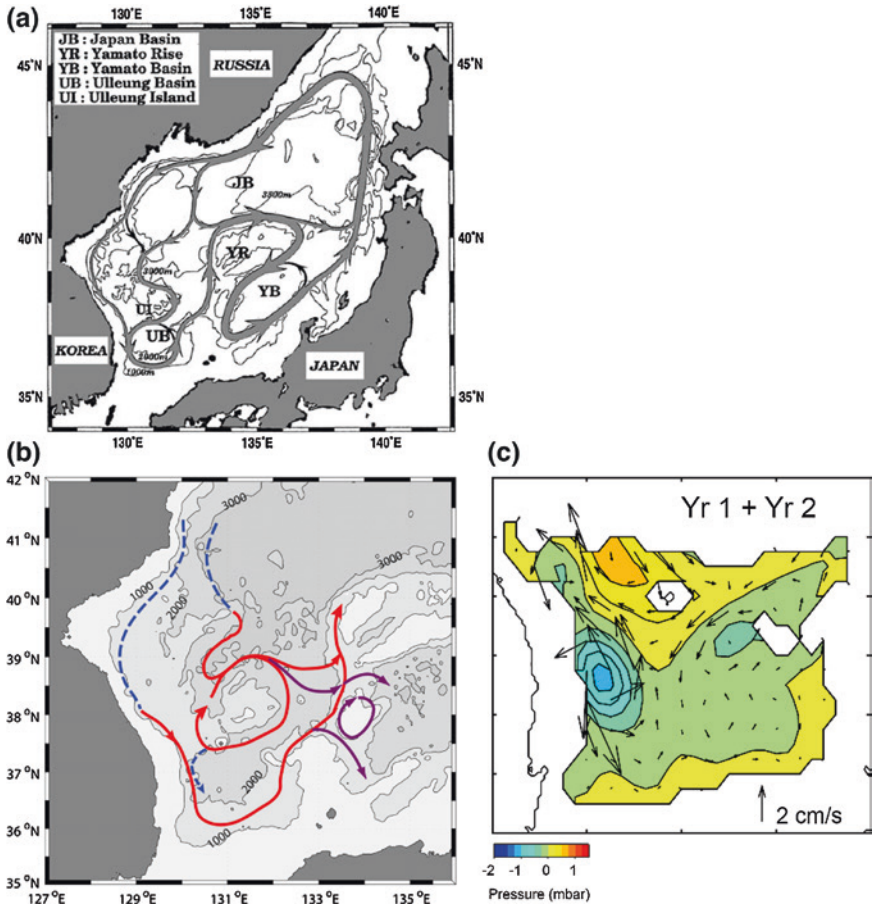

Fig. 4.8 Schematic deep circulation maps of **a** abyssal layer based on moored current measurements (from Senjyu et al. 2005), **b** 800 m layer based on trajectories of floats. *Red* and *violet lines* are drawn based on the float data, and *dotted lines* indicate the inferred continuation of subsurface currents (from Park et al. 2010), and **c** two-year average dynamic pressure field at 1000 dbar with corresponding geostrophic current vectors determined by bottom pressure and current measurements (from Teague et al. 2005)

cyclonic recirculation cells are found in the eastern JB and in the western YB (Choi and Yoon 2010; Park and Kim 2013). The deep circulation of the UB is complex with alternating cyclonic and anticyclonic sub-basin-scale cells (Fig. 4.8c) (Teague et al. 2005; Choi and Yoon 2010). Localized anticyclonic circulation at 800 m is found over the Korea Plateau (Park et al. 2004), seamounts over the Yamato Rise (Choi and Yoon 2010), and a seamount between Oki Bank and Yamato Rise (Choi and Yoon 2010) (Fig. 4.8b). Also observed is the flow at 800 m through a gap between the Oki Bank and the Yamato Rise, with mean volume transport of 1.83 Sv below 200 m according to numerical model results (violet solid arrows in

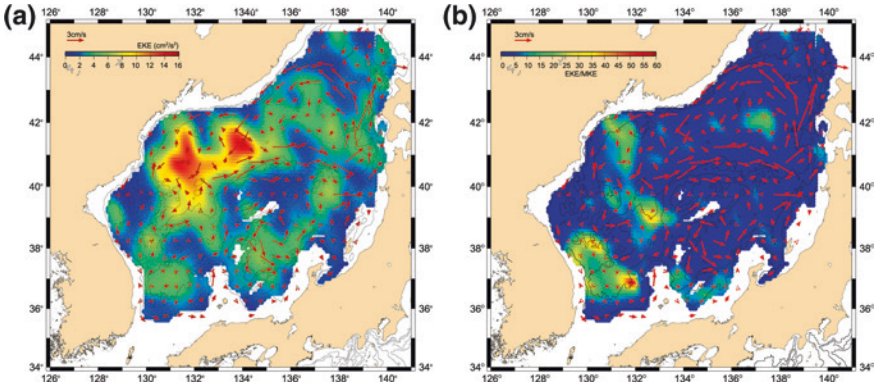

Fig. 4.9 0.5° × 0.5° bin-averaged currents at 800 m computed from float data compiled between 1999 and 2010. Superimposed (*color*) are **a** eddy kinetic energy and **b** ratio between eddy kinetic energy and mean kinetic energy, based on the same data (Redrawn from data provided by Dr. Jong-Jin Park)

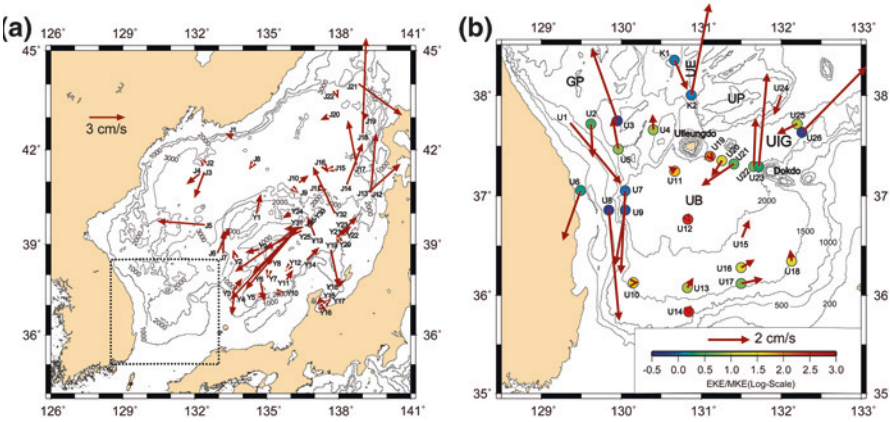

Fig. 4.10 **a** Mean abyssal currents based on long-term moored current measurements conducted in the Japan and Yamato basins between 1986 and 2007. **b** Expanded view of mean abyssal currents in the Ulleung Basin denoted by a *box* in (**a**). Ratio between eddy kinetic energy (EKE) and mean kinetic energy (MKE) in log scale is also shown as *colored dots* in (**b**). *GP*, *UB*, *UE*, *UIG*, *UP* denote Gangwon Plateau, Ulleung Basin, Ulleung Escarpment, Ulleung Interplain Gap, and Ulleung Plateau, respectively. For the detailed explanation of topographic features, see Sects. 1.1 and Chap. 16

Fig. 4.8b) (Park et al. 2010). It is argued that this throughflow in the gap is partly fed by the anticyclonic circulation over the Korea Plateau and an outflow from the UB (Park et al. 2010).

Space-time vector-averaged current in the entire East Sea based on float data at 800 m is about 2.5 cm s^{-1}, but mean current speeds in the strong recirculation cells reach 4–6 cm s^{-1} in the eastern JB and 7–8 cm s^{-1} in the western YB (Choi and Yoon 2010). The magnitude of deep currents at 800 m shows interbasin

differences, strongest in the JB and weakest in the UB (Choi and Yoon 2010; Park and Kim 2013) with maximum volume transports below 800 m (assuming no velocity shear below 800 m) in the JB, YB, and UB of about 10, 2.0, and 0.4 Sv, respectively (Choi and Yoon 2010).

Mean current speeds at deeper depths from mooring data range from 0.1 to 8.2 cm s^{-1} (Fig. 4.10), and strong currents with speeds higher than 4.0 cm s^{-1} were observed on the northwestern slope region of the YB (from Y26 to Y29) and the western slope region of the UB (U7, U8) which constitute the western boundary currents of the cyclonic circulation. The strong current on the eastern boundary of the JB (J18) is part of a deep cyclonic recirculation cell, and strong currents following the southeastern slope of the Ulleung Interplain Gap (UIG) (U23, U26) are due to the Dokdo Abyssal Current (DAC) (Chang et al. 2009). The Korea Plateau splits into the Ulleung Plateau to the east and the Gangwon Plateau to the west with the deep (>2000 m) and narrow (~10 km) Usan Escarpment in between (see Fig. 1.2 for topographic features in the UB). Moored current measurements at this passage (K2) show a relatively strong mean northward flow of about 4.5 cm s^{-1} (Baek et al. 2014), indicating that part of the deep water entering the UIG from the western JB bifurcates into two branches, one branch flowing back to the JB through the Usan Escarpment and the other branch entering the UB. A weak southward abyssal flow observed at K1, north of mooring K2, is thought to be due to the cyclonic penetration of abyssal waters near the northern side of the Usan Escarpment, according to Hogan and Hurlburt (2000). Over the Gangwon Plateau, northward abyssal currents are observed which correspond to the western rim of the anticyclonic deep circulation over the entire Korea Plateau (Park et al. 2004; Teague et al. 2005). At U1 and U2, a short distance to the west from the northward currents over the Gangwon Plateau, abyssal currents in a depth range of 800–1200 m show an opposite direction, south or southeastward. The southward deep currents at U1 and U2 are thought to originate from the area farther north, merging with the deep cyclonic circulation in the UB to form the strong western boundary current observed at U7 and U8. A mean southward current is also observed at around 450 m at U6 (Jang 2011).

Analysis of float data indicates that the deep currents generally follow potential vorticity contours (f/H contours, where f is the local Coriolis parameter and H is the depth.) in the JB (Choi and Yoon 2010). On the other hand, the topography-following characteristics of deep currents are less clear in the UB (Choi and Yoon 2010) and floats at 800 m tend to move toward shallower depths (Park and Kim 2013).

Evidence of cyclonic penetration of deep waters from the JB into the UB through the UIG was provided by both float data and moored current measurements (Park et al. 2004; Teague et al. 2005; Choi and Yoon 2010). Deployment of an array of five mooring across the UIG revealed that the abyssal flow through the UIG shows a two-way circulation, weak, broad southwestward flows in the western UIG and strong, narrow northward flows of the DAC in the eastern UIG (Chang et al. 2009). The mean speed of the DAC at 2000 m is about 7.9 cm s^{-1} with a maximum recorded current speed of about 33.9 cm s^{-1}. Kim et al. (2013)

showed that the DAC extends from the bottom up to 300 m depth, while the upper currents, above 200 m, flow to the south or southwest opposite to the DAC. While the inflow transport towards the UB through the UIG below 1800 m is about 0.15 Sv, the net volume transport is negligibly small with high temporal variability (Chang et al. 2009). It suggests an insignificant upwelling of deep water across the 1800 m depth level. On the other hand, other transport estimates from 250 m to the bottom or from 800 m to the bottom, based on numerical model results and float data, yielded a net inflow transport of about 0.3–0.4 Sv (Teague et al. 2005; Choi and Yoon 2010). The inflow transports below 250 m based on the models are estimated to be 0.68 Sv (Teague et al. 2005) and 1.0 Sv (Park et al. 2010). The formation rate of the East Sea Deep Water below 1500 m determined by box models constrained by chemical tracers (Postlethwaite et al. 2005; Jenkins 2008) is about 4–5 times smaller than the directly observed transport below 1800 m in the UIG, suggesting a different generation mechanism of deep currents besides that of deep water-formation (see Sect. 4.5.4) and implying that the water mass formation rate may not represent the strength of the East Sea THC.

4.4.2.2 Temporal Variability

While the mean speeds of deep currents range 0–8 cm s^{-1}, temporal variation of these currents is large and instantaneous current speeds reach as high as 30–50 cm s^{-1} below 2000 m (Takematsu et al. 1999a; Chang et al. 2009). EKE provides insights into the variability of currents, although it is often difficult to identify the source of variability. EKE from full-depth moored current measurements in the UB from about 40 m depth down to 1500 m or deeper ranges from 1.5 to 440 cm^2 s^{-2}, and it sharply decreases at around 300 m depth near the permanent pycnocline (Kim et al. 2009a, 2013; Jang 2011). EKEs of deep currents below the pycnocline computed from mooring data at discrete locations range from 0.8 to 19.7 cm^2 s^{-2} with the ratio between EKE and mean kinetic energy (MKE) ranging from 0.5 to 497 in the UB (Chang et al. 2002, 2009; Teague et al. 2005; Kim et al. 2013). EKE of deep currents in the JB shows a similar range (Takematsu et al. 1999a). In the UB, low EKE/MKE ratios occur in regions of strong mean currents such as the DAC (U25, U23), on the western continental slope (from U7 to U9), over the Korea Plateau where the strong anticyclonic circulation exists (U3), and in the Ulleung Escarpment (K2) (Fig. 4.10b).

While the surface EKE based on surface drifters is low in the JB, except in a narrow band along the Primorye coast, EKE computed from the float data within 0.5° bins at 800 m exhibits the highest EKE (~15 cm^2 s^{-2}) in the western JB (Fig. 4.9a) where a strong dipole structure of wind-stress curl in winter is located (Park and Kim 2013). Apart from the western JB, EKEs are generally high (~5 cm^2 s^{-2}) in the interior of the UB and YB, and the eastern JB where mean currents are weak. The EKE/MKE ratio from the float data shows a high ratio in the UB and along the boundary of the dipole wind-stress curl in winter (Fig. 4.9b).

Moored current measurements in the East Sea show a distinct seasonal variation of deep currents in the JB (Takematsu et al. 1999a) with maximum velocities (~4.4 cm s^{-1}) in March and April and a minimum in November (~2.3 cm s^{-1}) (Choi and Yoon 2010). The estimation of monthly mean velocities at 800 m using the float data from the JB also shows a clear seasonal signal with a maximum (~3.5 cm s^{-1}) in March and a minimum in November (~2.3 cm s^{-1}) (Choi and Yoon 2010). On the other hand, mooring data indicate that the seasonal variability of deep currents is not obvious in the UB and YB, showing double current speed maxima, one in January and the other in July/August (Chang et al. 2002; Choi and Yoon 2010). The monthly mean velocities from float data at 800 m in the UB and YB also show reduced annual amplitude with poorly defined seasonal variation in the UB and YB (Choi and Yoon 2010).

The integral time scale of the measured deep currents ranges from 3 to 30 days, indicating the dominant time scales of deep current fluctuations. Intraseasonal variability of deep currents has been documented in the UB (Chang et al. 2002, 2009; Kim et al. 2013) with a period range of 10–60 days, and also in the YB with a shorter timescale of 2–10 days (Senjyu et al. 2005). Kim et al. (2013) showed that the variability of the DAC in the eastern UIG on timescales of 10–20 days is consistent with the propagation of topographic Rossby waves associated with warm events in the upper layer resulting from eddying processes and/or meandering of the TWC.

4.5 Dynamical Aspects

4.5.1 How Is the Tsushima Warm Current Driven?

The question of how the TWC is driven has long been an interesting theoretical problem. There are some studies showing that volume transport of the TWC is related to sea level difference between the interior and exterior of the East Sea (Toba et al. 1982; Ohshima 1994; Tsujino et al. 2008). On larger spatial and temporal scales, the TWC can be thought of as linked essentially to the wind-driven ocean circulation in the North Pacific, outside the East Sea. This idea was first explored by Minato and Kimura (1980). They considered a barotropic, linear dissipative, wind-driven ocean connected on the west to a shallow marginal sea through narrow inflow and outflow channels, and successfully showed that the transport through the marginal sea is driven by the large-scale wind field. However, the resulting volume transport was greatly overestimated because of many simplifications. The most serious of these may have been the neglect of the large barrier effect arising in the shallow inflow and outflow channels. In a similar way, Nof (1993) considered the same problem as one of geostrophic adjustment of buoyant Kuroshio water injected through a narrow gap into the marginal sea filled with deep, motionless denser water. Later, he also considered various other models applicable to the TWC (Nof 2000): a one-and-a half layer

numerical model (Bleck and Smith 1990), Godfrey's island rule (Godfrey 1989), and Nof's (1993) β-controlled formula. All these models, except for the island rule, are non-linear and neglect the barrier effect. They all give a transport of about 10 Sv, much larger than the measured value of about 2.5 Sv (Teague et al. 2002; Takikawa et al. 2005; Fukudome et al. 2010). These studies indicate that non-linear effects are not important in controlling the volume transport through the marginal sea. Instead, the overestimation of volume transport may be induced by the neglect of the barrier effect arising in shallow channels, as it is in the study of Minato and Kimura (1980). Indeed, Seung (2003) has obtained a transport of about 2.5 Sv by applying the island rule, taking a bottom friction into account with a reasonable bottom friction coefficient. Hence, he parameterizes the barrier effect simply as bottom friction. According to Yang et al. (2013), the barrier effect includes the form drag associated with bottom pressure torque, generation of cross-isobathic flow by horizontal friction, and northward shifting of the forcing region affecting the through flow. All these facts indicate that the TWC is essentially driven by the oceanic wind field, and its volume transport is largely controlled by the barrier effect arising in the inflow and outflow channels. In fact, it can be understood that the downstream sea level drops occurring in the inflow and outflow channels are consequences of the barrier effect. Zheng et al. (2010), however, suggest a different view that the TWC becomes stronger and flows closer to the Japanese coast as the Kuroshio becomes stronger, based on a numerical experiment.

The volume transport of the TWC undergoes a seasonal variation with maximum in summer-fall and minimum in winter (Teague et al. 2002; Takikawa et al. 2005; Fukudome et al. 2010). An interesting feature about it is that the seasonal variation of outflow volume transport appears to be larger in the Soya Strait than in the Tsugaru Strait (Nishida et al. 2003; Fukamachi et al. 2008). This problem is addressed by Seung et al. (2012) with a simple linear barotropic model. As in the steady problem, they use the island rule with bottom friction taken into account. In the steady problem, only one outflow channel with only one island is considered. The island rule with multiple islands and multiple frictional channels gives somewhat different results from the case with a single island and two channels. They show that the volume transport through a channel is determined not only by the circulation around the adjacent two islands created by the oceanic wind field off those islands, which is the case if there is no bottom friction, but also by those around the neighboring islands further away. Note that the latter does not occur if only one island (two channels) is considered, even in the presence of bottom friction. Hence, the volume transport through each channel (strait) of the East Sea is determined by a linear combination of two components of circulation: one is the circulation around Honshu/Kyushu created by the oceanic wind field east of Honshu/Kyushu, and the other is the circulation around Hokkaido created by the oceanic wind field east of Hokkaido. For example, the transport through the Tsugaru Strait (Q_{23}) is the sum of two components $Q_{23,12}$ and $Q_{23,34}$ associated, respectively, with the wind fields off Honshu/Kyushu and Hokkaido (Fig. 4.11). In the same manner, the transport through the Soya Strait (Q_{45}) is the sum of the

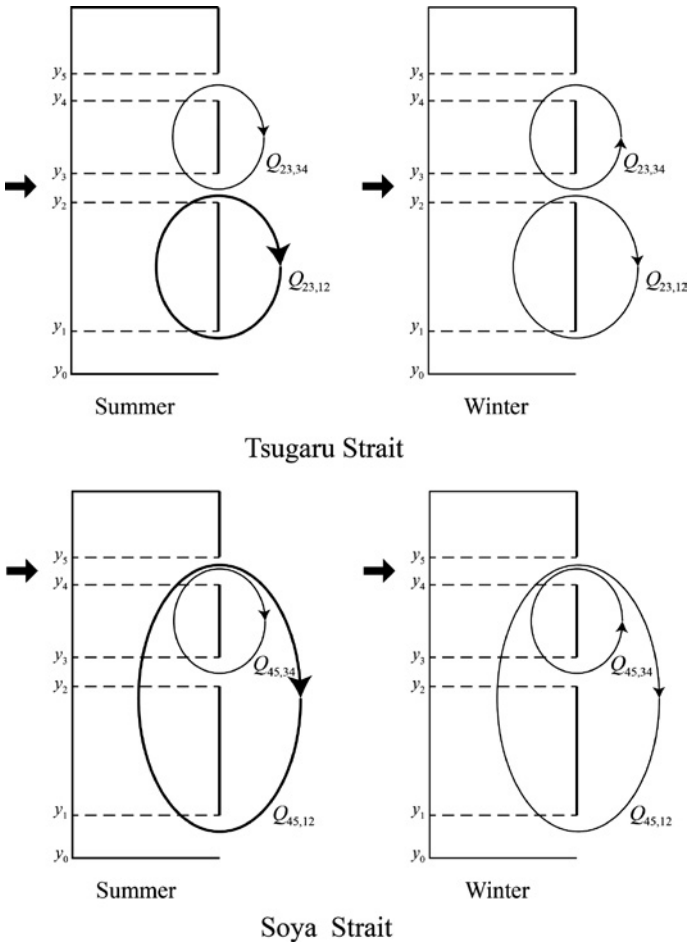

Fig. 4.11 Formation of volume transports through the Tsugaru and Soya Straits (*thick horizontal arrows*) in summer and winter by the circulations (*arrowed circles*) induced by wind fields off Honshu/Kyushu ($Q_{23,12}$ for Tsugaru Strait and $Q_{45,12}$ for Soya Strait) and Hokkaido ($Q_{23,34}$ for Tsugaru Strait and $Q_{45,34}$ for Soya Strait). The *arrowed circles* $Q_{23,12}$ and $Q_{45,12}$ are thicker in summer than in winter because they are larger in summer than in winter (from Seung et al. 2012)

two components $Q_{45,12}$ and $Q_{45,34}$ (Fig. 4.11). According to the model, the different behavior in seasonal variation of volume transports between the Tsugaru and Soya Straits is due essentially to the fact that the wind-stress curl off Hokkaido changes its sign from negative in summer to positive in winter, the latter fact being associated with the large seasonal fluctuation of zero-stress-curl latitude east of Hokkaido.

4.5.2 How Are the Branches of the Tsushima Warm Current Formed?

As described in Sect. 4.1, the TWC has traditionally been believed to split into three branches after entering the East Sea: the Nearshore Branch, the Offshore Branch, and the EKWC. In a series of numerical experiments, Yoon (1982a, b) has found that the EKWC is formed by western intensification and the Nearshore Branch is constrained by shallow bottom depth to flow along the Japanese coast. Later, Kawabe (1982) has shown that the Offshore Branch is induced by the coastally-trapped waves associated with the seasonal variation of TWC volume transport. It is already noted in Sect. 4.1 that the Nearshore and Offshore Branches are not usually identifiable separately and instead there seems to be only one broad current especially notable in summer, referred to as the Eastern Branch (Fig. 4.1). The hypothesis that the EKWC is a western boundary current is problematic in explaining formation of the Eastern Branch and seasonal variability of the EKWC which is strongest in summer and weakest in winter (cf. Lee and Niiler 2010a). Suppose that the EKWC is a western boundary current; then, seasonal variability of the EKWC requires that Rossby waves cross the East Sea basin very quickly, in a time shorter than a few months, which is not possible. Also, the Eastern Branch cannot exist if any pressure disturbance on the eastern boundary propagates westward by Rossby waves and hence disappears. The hypothesis of topographic trapping is possible, but it will be limited to a very narrow Japanese coastal region where the isobaths are discontinuous at some locations. The questions that follow are about how the EKWC and the Eastern Branch are formed and how their seasonal variabilities arise.

Recently, Spall (2002) has proposed an idea that the Eastern Branch is induced by the buoyancy difference between TWW and the other water in the East Sea, although he does not consider the seasonal variability. The buoyancy of the TWW is carried along the Japanese coast relatively quickly by Kelvin waves. It is trapped along the coast by the effect of local thermal damping, and would otherwise be propagated westward by Rossby waves. Hence the Eastern Branch can be present in both deep offshore and shallow coastal areas. This idea may be extended further in explaining the seasonal variations of the EKWC and the Eastern Branch if we take the local buoyancy forcing into consideration as an additional factor, as shown by Seung and Kim (2011). In the latter model, the East Sea basin is subject to seasonally-varying local buoyancy forcing, with larger buoyancy in summer than in winter, while the western and eastern boundaries are respectively affected by less buoyant water originating from the north and more buoyant water originating from the south. Hence, this model indicates that the seasonal variation of the EKWC and the Eastern Branch is induced by both local and remote buoyancy forcing.

It can be argued that the EKWC is driven by the inertia of the TWC incident upon the East Sea basin with seasonally-varying strength. In order to demonstrate this possibility, Seung (2005a) has considered an incident inertial jet initially in

contact with the bottom and injecting into a deep basin by crossing a depth discontinuity. The grounded portion changes its flow direction being trapped over the shallow bottom while the ungrounded portion continues to flow by virtue of the inertial effect, hence resulting in the branching. Arruda et al. (2004) also share the same view in explaining the formation of the UWE. Eddies are usually expected to migrate due to the β-effect and to be advected by mean currents. Hence, the quasi-stationary characteristics of the UWE had long been an enigma. According to Arruda et al. (2004), the UWE owes its presence to the force balance in the area surrounding it. The stationary UWE exerts a southward force, referred to as β-induced force, because of latitudinal difference of the Coriolis force arising from the flow within the UWE. This β-induced force is balanced by the northward inertial force exerted by the TWC injecting into the East Sea basin. Hence this study presumes that the EKWC results from the inertia of the injecting TWC.

There are some other studies suggesting that the branching is locally triggered. Cho and Kim (2000) have proposed an analytical model suggesting that branching is caused by the creation of negative vorticity induced by intrusion of the Korea Strait Bottom Cold Water (KSBCW) along the western side of the Korea Strait in summer (see Chap. 3). Ou (2001) has shown that two current axes, one along the coast and the other along the outcrop of the buoyant layer, are generated when a single-axis current enters a deep basin after passing through a shallow channel subject to bottom friction. Both observations (Teague et al. 2002) and fine-resolution numerical models (e.g. Kim 2007) show that the branching begins just south of Tsushima Island, indicating that the branching mechanism is more or less similar to that of a jet split by an obstacle. An interesting question that follows is how far such locally-triggered branching is maintained under the effect of Earth's rotation. In conclusion, the dynamics associated with formation of the TWC branch currents are not yet definitely clear.

4.5.3 What Is the Role of Local Forcing?

The East Sea is strongly affected by local forcing, both of wind and buoyancy (Hirose et al. 1996; Yoon and Kawamura 2002). Strong northwesterly winds prevail in winter. At some locations, such as off Vladivostok, winds are orographically funneled becoming stronger than elsewhere (see Chap. 2). Such strong outbreaks of cold and dry continental air cause intense surface cooling that can lead to deep water formation (Seung and Yoon 1995a), as well as small-scale intense wind-stress curl. In the warm-water region, the behavior of the surface currents carrying TWW depends mostly on the volume transport through the inflow opening, whereas in the cold-water region, the current forms a closed cyclonic circulation, as observed by Isobe and Isoda (1997), with its strength depending on the magnitude of local forcing, as numerically demonstrated by Hogan and Hulbert (2000). Indeed, a simple linear analytical model proposed by Seung (1992) seems to be revealing. In the presence of inflow and outflow alone, western

intensification predominates and most of the basin looks like the warm-water region. In the presence of local forcing alone, the basin-scale cyclonic gyre predominates and the whole basin looks like the cold-water region. This is because the local wind stress curl is generally positive and local surface cooling induces a vortex stretching of the upper layer. In the presence of both effects, the inflow-outflow and the local forcing, there appears a front separating the warm-water and cold-water regions in such a way that the two effects compete with each other. The relative importance of one effect compared to the other determines the separation latitude and the position of the front. In this simple model, however, the Eastern Branch does not appear because both bottom topography and buoyancy difference between TWW and the basin water are ignored. Additionally, it is questionable whether the local wind forcing in the cold-water region can induce any circulation intruding beneath the surface currents through the mechanism of ventilation proposed by Luyten et al. (1983). This problem has been addressed by Seung (1997) with the conclusion that the wind-forced circulation indeed pushes the lateral boundary of the surface currents southward, in agreement with the results described above, but hardly intrudes beneath the surface currents. Nevertheless, this study does not consider bottom topography, which may be an important factor in determining the circulation underlying the surface currents.

4.5.4 How Is the Deep Layer Circulation Driven?

As described in Sect. 4.3, the deep circulation flows cyclonically along the isobaths, often shows oscillatory and eddy-like features, is stronger in winter than in summer in the JB, and occasionally becomes stronger after an event of deep water formation. Holloway et al. (1995) have attempted to explain the formation of deep currents in terms of the eddy-topography interaction, the so-called Neptune effect. However, the results depend strongly on the parameterization coefficient of the interaction. On the other hand, Hogan and Hulbert (2000) have suspected that baroclinic instability is a candidate mechanism for deep current generation, although it was not explicitly shown to be so in their numerical experiments. In these explanations, the energy of deep currents is assumed to come ultimately from disturbances generated in the upper layer, and any effect of buoyancy forcing, such as deep water formation, is ignored. Recent numerical experiments (e.g. Kim 2007) with horizontal resolution comparable to, but vertical resolution more refined than, that of Hogan and Hulbert (2000) give nearly the same pattern of deep currents as that observed. However, the numerically obtained deep currents appear much weaker than those observed. It seems that numerical models are not yet complete enough to reproduce either the process of downward momentum transfer or realistic deep water formation. Based on the fact that most geostrophic contours are closed on themselves in the deeper part of the East Sea and that even weak forcing can generate strong abyssal currents over the closed geostrophic contours (Rhines and Young 1982), Seung (2005b, 2012) has discussed

the possible roles of wind and deep water formation in generating deep currents. In winter, vertical stratification becomes very weak in some areas by intense surface cooling. If these areas, though not large, are over the closed geostrophic contours, the surface wind may be effective in generating deep currents (Seung 2005b). Deep water formation is equivalent to a volume source and can give rise to a source-driven circulation in the deep layer. If this happens in an area of sloping bottom, the pressure disturbances associated with the volume source propagate rapidly as topographical waves along the isobaths, resulting in deep currents (Seung 2012). However, it is known that the intensity of deep water formation has been decreasing in recent decades (e.g. Gamo et al. 2001; Kim et al. 2004a), implying that the resulting convection is not deep enough, while the deep currents are still present. Yoshikawa (2012) has addressed this problem with an idealized numerical model. He considers a three-layer ocean with sloping bottom, and supposes that winter convection reaches only to the intermediate layer. In the bottom layers, there still occurs a cyclonic circulation along the isobaths, created by the interaction between eddies generated during the process of water mass conversion and bottom topography. The strength of the circulation is found to depend on the volume of water mass conversion. This study indicates that deep water formation is the most probable candidate for the generation of deep circulation, although the detailed mechanism of it is not yet completely clear. Recently, Park et al. (2013) suggest that geothermal heating, being about twice that of a typical abyssal plain, is yet another possible candidate driving force for the deep circulation.

4.6 Numerical Modeling Studies of Circulation

4.6.1 Numerical Simulations

Early versions of realistic numerical models were configured on the Arakawa B-grid which gives better performance when the horizontal resolution is coarse. Seung and Kim (1993) applied Cox's (1984) model to simulate the circulation in the East Sea. Its horizontal grid size was 0.2° in both latitude and longitude and the number of vertical grid cells was 23, which was a high resolution model for that time. Surface temperature and salinity were restored by observed values from the Japan Oceanographic Data Center. The model was forced by surface wind stress from Na et al. (1992) and by constant inflow and outflow. At the open boundary, salinity and temperature were nudged by observed values from the National Fishery Research and Development Institute of Korea. Typical features of the circulation in the East Sea, such as the Nearshore Branch, EKWC, NKCC and so on, were reproduced in this model.

Seung and Kim (1997) applied the Miami Isopycnic Coordinate Ocean Model (MICOM; Bleck et al. 1992) to estimate the time scale of renewal of the upper intermediate water in the East Sea. Though their model has low horizontal resolution of 0.5° and only 4 vertical layers, it is noteworthy in applying an isopycnic

coordinate model for the first time with realistic meteorological forcing and open boundary conditions. They investigated the formation of intermediate and deep waters and could estimate that the renewal timescales for upper intermediate water and for the whole water mass are about 10 and 81.4 years, respectively. From their numerical study, the renewal timescale for the whole water mass is comparable to that of Kim and Kim (1996) based on their moving box model and observations.

Kim and Seung (1999) also applied the MICOM but increased the horizontal resolution to 0.2° and vertical layers to 10 to investigate the formation and movement of East Sea Intermediate Water (ESIW). They resolved realistic surface currents in the East Sea such as the TWC and the separation of the EKWC. In particular, they reproduced the formation of ESIW by winter convection off Vladivostok and its southward extension along the Korean coast into the UB.

With the Geophysical Fluid Dynamics Laboratory Modular Ocean Model Version 2 (GFDL-MOM2) *z*-coordinate model, Kim and Yoon (1999) set up a relatively high resolution numerical model with horizontal resolution of 1/6° and 19 vertical levels forced by seasonally varying inflow and outflow, monthly mean meteorological wind stresses, Haney-type heat flux, and restored freshwater flux. They resolved well the surface and intermediate circulations in the East Sea in terms of seasonal variation as well as the mean features of the Nearshore Branch, EKWC, and NKCC. It is noteworthy that Kim and Seung (1999) and Kim and Yoon (1999) could reproduce the general circulation of the East Sea comparable to the observed one. Those models had higher resolution than the previous numerical models, and reproduced the branching of the TWC and suppressed separation of the EKWC to the south of 38°N, in agreement with observations. In particular, both models resolved intermediate waters in the East Sea such as the NKCC and ESIW in terms of their formation and extension.

Yoon and Kawamura (2002) applied the same model as that of Kim and Yoon (1999) except using the European Centre for Medium-range Weather Forecasts (ECMWF) wind forcing which resolves a more realistic dipole structure for the wind stress curl produced by the orographic effect off Vladivostok. Their model resolved the ESIW, UJSPW, and the High Salinity Intermediate Water although its salinity was lower and its temperature higher than the observed values. In particular, the model results suggested that UJSPW is formed off Vladivostok by deep convection in winter and is advected by the current near the base of the convection to intrude below the ESIW layer.

A model intercomparison experiment was conducted by Lee et al. (2003a) between RIAM Ocean Model (RIAMOM; Lee and Yoon 1994) and Geophysical Fluid Dynamics Laboratory Modular Ocean Model (GFDL MOM1, version 1.1). Their work was the first intercomparison study of East Sea circulation models, although only two models may not be enough to assess the models' performances. Basically, the two models have similar numeric schemes such as assuming hydrostatic and Boussinesq approximations, applying the Arakawa B-grid system, and so on, but RIAMOM has a free surface while MOM assumes a rigid-lid without a free surface. Both models have the same horizontal grid size of 1/6° and the same 19 uneven vertical levels and were forced by the monthly mean inflows

and outflows, Haney-type heat flux, and monthly mean wind stresses from the reanalyzed ECMWF data. Although both models successfully reproduced the general circulation features of the East Sea, such as the Nearshore Branch, EKWC, and NKCC, they showed a tendency to overestimate (underestimate) temperature (salinity) below 50 m compared to the observed values of the Generalized Digital Environmental Model (GDEM) climatology. Nevertheless, it was shown that RIAMOM has better performance in producing a realistic East Sea flow field.

Coarse resolution models have had trouble reproducing the general circulation of the East Sea, particularly, the overshooting of the EKWC. To resolve this defect of the models, Holloway et al. (1995) introduced "topostress" to parameterize the eddy-topographic interaction in the East Sea which was poorly resolved in the coarse resolution models. They used the Modular Ocean Model (MOM, Pacanowski et al. 1991) which is very similar to that used by Seung and Kim (1993). Its horizontal resolution was 1/5° and the number of vertical levels was 25. By exploring sensitivity to an eddy parameter, the general circulation in the East Sea was improved, and in particular the overshoot of the EKWC was reduced or eliminated, bringing results close to the observations in the East Sea. It is interesting to compare their results with Hogan and Hurlburt's (2000) exploration of sensitivity to horizontal resolution, which will be introduced next.

With realistic configurations of the East Sea, a few experiments have been conducted on model sensitivities to horizontal resolution and mixing parameterization. Hogan and Hurlburt (2000) investigated numerical performance in reproducing the East Sea surface circulation, in relation to horizontal resolution and bottom topography by applying the Naval Research Laboratory's Layered Ocean Model (NLOM). In particular, it is noteworthy that Hogan and Hurlburt (2000) applied, for the first time, an Arakawa C-grid model which gives better performance in high horizontal resolution models (Haidvogel and Beckmann 1999). Hogan and Hurlburt (2000) demonstrated the sensitivity of the circulation in the East Sea to various horizontal grid sizes from 1/8° to 1/64°. In addition, the impacts of the bottom topography and surface wind forcing were discussed. From various simulations, they recommended that the high resolution model with at least 1/32° horizontal grid size is required to resolve the realistic separation of the EKWC from the Korean coast and to generate sufficient baroclinic instability to produce eddy-driven cyclonic deep mean flows. Their results also suggest that the separation latitude of the EKWC depends on the spatial structure of the wind stress curl and bottom topography as well as the model's horizontal grid size. In particular, the problems of EKWC overshooting and too-weak deep circulation, which are commonly noted in previous numerical studies in the East Sea, were discussed in this study. The sensitivity to the surface wind stress forcing was presented by Hogan and Hurlburt (2005) in more detail. Hogan and Hurlburt (2006) applied Hybrid Coordinate Ocean Model (HYCOM) with a 1/25° horizontal grid and 12 layers to reproduce the intra-thermocline eddies reported by Gordon et al. (2002) in the East Sea and suggested three mechanisms for the formation of those eddies.

Lee et al. (2011) conducted a sensitivity experiment to study tidal effects on intermediate waters in the East Sea. They applied the RIAMOM, improving the

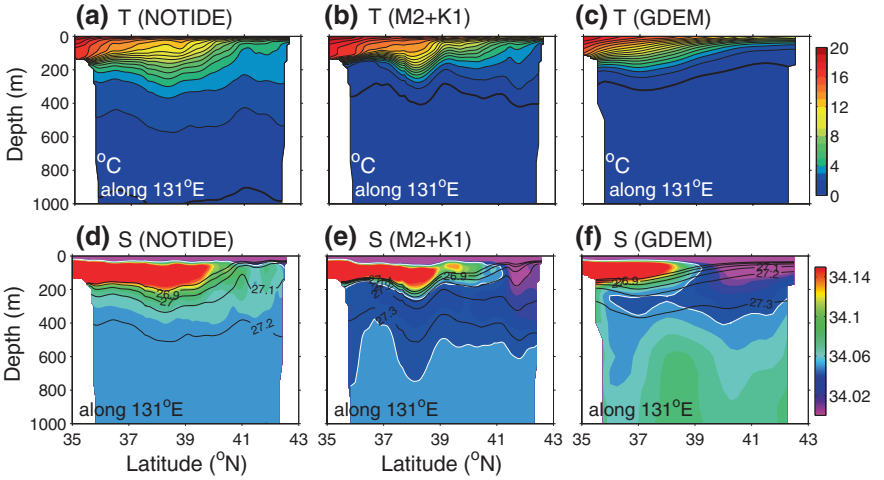

Fig. 4.12 The meridional section of potential temperature along 131°E for **a** without tide, **b** with M_2 and K_1 tides, and **c** the GDEM climatology. Contour interval is 1.0 °C, and thick contours indicate 1.0 °C. **d–f** corresponding salinities at the same section. Contour interval is 0.01, and *white contours* indicate S = 34.05 psu. The *solid contours* indicate isopycnal layers from $\sigma_\theta = 26.8$ kg m^{-3} to $\sigma_\theta = 27.3$ kg m^{-3} with an interval of 0.1 kg m^{-3} (from Lee et al. 2011)

horizontal grid resolution to 1/12° and increasing the number of vertical levels to 50, compared to 1/6° and 19 levels used by Lee et al. (2003a). Their study showed that direct inclusion of tide-induced processes significantly improves the representation of intermediate water mass properties and circulation in the East Sea. Figure 4.12 shows that the case with tides reproduces well the main ESIW features on the meridional section along 131°E. In addition, the domain-averaged temperature and salinity biases in their model were reduced considerably and the wind-driven southwestward flow along the coastline in the upper layer was enhanced, because of tidal mixing and internal tide processes. Their results represent the first approach to a discussion of tidal effects on the East Sea circulation.

Recently, numerical models in the East Sea have advanced to produce results comparable to observations. Luneva and Clayson (2006) and Clayson et al. (2008) simulated deep convection in the East Sea during the winters of 1999–2000 and 2000–2001 with an eddy-resolving model having high horizontal resolution. They used the University of Colorado version of the Princeton Ocean Model (POM; Kantha and Clayson 2000) with 6 km horizontal resolution and 38 depth levels (11 sigma levels in the upper 100 m and 27 z-levels at the shelf break and in the deep sea). They showed realistic surface and deep circulations, comparable with the observed surface and deep circulation reported by Lee and Niiler (2005), Takematsu et al. (1999a), Senjyu et al. (2005), and Teague et al. (2005). In particular, these studies attempted to explain the observed characteristics of the deep East Sea circulation by numerical modeling. Luneva and Clayson (2006) analyzed the effect of seasonal surface flux variability on the abyssal current and a possible

mechanism for a weakening of the bottom drag coefficient due to turbulent mixing during the winter ventilation of the East Sea. Using the same model, Clayson et al. (2008) suggested that a vertical coupling between the upper and lower circulations can enhance deeper mixing through downwelling in a localized region.

Most numerical models, including those with realistic configurations, have assumed the hydrostatic approximation. To study the dynamics of the subpolar front in the East Sea, however, Yoshikawa et al. (2012) adopted a non-hydrostatic numerical model. Since the non-hydrostatic model computes vertical motion dynamically, it can represent the effect of wind stress and surface cooling on ageostrophic vertical motion and frontal subduction at the frontal region. Though the model employed a simple configuration with a rectangular domain and flat bottom, its results reproduced vertical motion by wind-generated internal gravity waves and subduction by surface cooling, which were confirmed by comparing with observational results (Lee et al. 2006)

4.6.2 Data Assimilation and Forecasting Systems

Over the last decade, interest in ocean forecasting systems has grown with increase in computing power as well as improving ocean observing systems such as satellites, Argo, CREAMS programs, and so on (see Chap. 1). Ocean data assimilation has been regarded as an essential technique in developing an ocean forecast system, since it initializes the ocean model with a sufficient amount of available data, thereby improving the forecasting performance. Ocean data assimilation also provides diagnostic tools for understanding oceanic and climatic conditions.

Initially, ocean data assimilation was applied to the East Sea by introducing nudging terms to the 3 dimensional temperature and salinity fields to reproduce realistic circulations and allow investigation of intermediate water formation and circulation processes (Seung and Yoon 1995b; Yoshikawa et al. 1999).

Hirose et al. (1999) applied the approximate Kalman Filter (Fukumori and Malanotte-Rizzoli 1995) to assimilate TOPEX/Poseidon altimeter data into a 1.5-layer, reduced gravity model. The formulation of the model is the same as that of Kim and Yoon (1996). The horizontal grid resolution is 1/6°. Though it is not a 3-dimensional model, it was a first attempt to apply a data assimilation technique. It was shown that their model was improved by data assimilation method, especially south of the subpolar front. The approximate Kalman Filter was also applied to the RIAMOM by Hirose et al. (2007) to develop an operational forecasting system for the East Sea. The model configuration is similar to Lee et al.'s (2011) eddy-resolving model but the number of vertical levels is 36. The model is forced by realistic in/outflow and daily meteorological forcing from the ECMWF. Temperature and salinity at the boundary are taken from the results of You and Yoon's (2004) 1/6° Pacific Ocean model while the velocity is diagnosed from the density field by the thermal wind relationship under the constraint of total volume transport in the Korea Strait measured by a ferryboat ADCP (Takikawa

et al. 2005). Satellite measurements of SST and sea surface height (SSH) were assimilated into the model while surface salinity was restored to the climatological monthly mean. It was shown that their data assimilation system improves subsurface mesoscale variability as well as surface circulation in the East Sea. It is remarkable that averaged root-mean-square SST error between their best estimates and the radiometer data is only 1.2 °C.

Kim et al. (2009b) implemented a three-dimensional variational method (3D-Var; Weaver and Courtier 2001) to an East Sea circulation model. They adopted GFDL-MOM3 for their eddy-resolving circulation model of the East Sea. The longitudinal horizontal grid varied from 0.06° at the western boundary to 0.1° in the east of 130°E in order to resolve a realistic EKWC, but latitudinal grid spacing was fixed to 0.1°, and the number of vertical levels was 42. Surface heat flux was calculated by the bulk formula with realistic meteorological variables from ECMWF, while the surface salinity was restored to the observations from the World Ocean Atlas. For the velocity through the Korea Strait, the barotropic velocity was given by the volume transport monitored by a submarine cable (Kim et al. 2004b). Satellite measurements of SST and SSH anomaly were assimilated, together with temperature profiles, into the model. Through comparison between model results and observations, it was shown that the assimilation system enables the model to reproduce realistic mesoscale eddy variability such as the UWE and the DCE as well as the mean circulation of the East Sea (Fig. 4.13). In particular, seasonal variation of the NKCC was well reproduced: a strong southward NKCC in summer and its weakening in winter, consistent with results from hydrographical observations (Kim and Kim 1983).

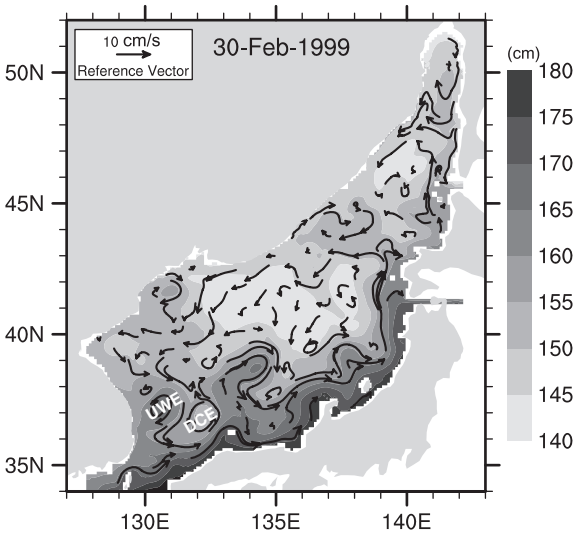

Fig. 4.13 Snapshot of sea surface height and currents on 24 February 1999 produced by a 3-dimensional variational data assimilation system. *UWE* and *DCE* respectively denote the Ulleung Warm Eddy and Dok Cold Eddy (Redrawn from Kim et al. 2009b)

Recently, numerical models of the East Sea, incorporating the data assimilation technique, have advanced to become operational ocean forecast systems. RIAMOM (Hirose et al. 2007) has already been applied to the East Sea operational ocean forecast system for the first time in the East Sea, which is available online (http://dreams-i.riam.kyushu-u.ac.jp/vwp/html/model_info.html).

4.7 Summary and Discussion

Various direct observations using satellite technology in the southern East Sea have revealed new near-surface circulation features. The EKWC and Nearshore Branch, after respectively leaving the coasts of Korea and Japan, join in the area east of the UB and form a broad mean current system named the East Sea Current (Lee and Niiler 2005). The East Sea Current, which exits the East Sea through the Tsugaru Strait, is well reproduced by numerical models (e.g. Clayson et al. 2008) and by an analytical solution in a simplified box model of the East Sea (Arruda et al. 2004). The Nearshore Branch, which is historically described as an alongshore current following the coast of Japan from the eastern channel of the Korea Strait to the Tsugaru Strait, is only observed in the summer season (May–August). The path of the flow passing through the western channel of the Korea Strait is found to be determined by the vorticity of the flow before entering the East Sea and branching of the current only occurs less than 15 % of the time. A reversal of the NKCC is also observed, and a southward alongshore NKCC is only observed during summer months (May–August). But these observations of NKCC are based on statistically insufficient drifter observations in the area due to deployment difficulties near North Korea.

It is found that eddies in the southern East Sea congregate in meridional bands determined by the sign of the mean flow vorticity, i.e. the anticyclonic and cyclonic eddies are born, grow, propagate and decay in the mean negative vorticity band and in the mean positive vorticity band, respectively. A relatively high number of anticyclonic eddies in the UB (negative vorticity zone) are found to have life spans longer than one year, being sustained by receiving kinetic energy from the meandering mean flow.

After its formation in the JB, deep water circulates cyclonically in the JB, and part of it penetrates cyclonically into the southern UB and YB through abyssal channels and gaps (Senjyu et al. 2005; Chang et al. 2009). Hence, the deep circulation of the East Sea is characterized by cyclonic circulation in each of the deep basins with strong currents of 4–8 cm s^{-1} along the perimeter of each basin and sluggish flows of 1–3 cm s^{-1} in the basins' interiors. Deep circulation in the UB is weakest and highly variable with alternating cyclonic and anticyclonic subbasin-scale cells. Strong cyclonic recirculation cells with spatial scales of about 200 km exist in the eastern JB and the western YB. Deep currents in the JB show

a distinct seasonal cycle with their respective maximum and minimum speeds in March and November. The seasonal variation of currents, however, is not obvious in the UB and YB. Instead, energetic temporal variability on timescales of 5–60 days is dominant.

The East Sea circulation is classified into two regimes: upper-layer circulation generated by bifurcation of the TWC entering the basin, and deep-layer circulation driven by local forcing and isolated in the basin. Most studies agree that the TWC is essentially driven by the oceanic wind field in the North Pacific, and its volume transport is largely controlled by the barrier effect arising at the inflow and outflow channels. The different behavior in seasonal variation of volume transports in the Tsugaru and Soya straits has been ascribed to sign changes of the wind stress curl off Hokkaido (it changes from negative in summer to positive in winter, due to the large seasonal fluctuation of the zero-stress-curl latitude east of Hokkaido), although there are not yet enough studies supporting this explanation. The formation mechanisms of the EKWC and the Eastern Branch, both being branch currents of the TWC, are diverse, as reviewed in Sect. 4.5.2. There is an indication that seasonal variation of the EKWC and Eastern Branch is due to the combined effect of local and remote buoyancy forcing, although this explanation does not find further supporting studies. There are many studies suggesting that the upper-layer circulation in the cold-water region is susceptible to local wind and buoyancy forcing, which are favorable for a basin-wide cyclonic gyre.

In the early phase of numerical studies in the East Sea, idealized simple models were introduced. Though those simple models did not simulate realistic circulations in the East Sea, they have provided valuable tools for understanding the dynamics of the East Sea circulation. With the advance of computational power, it has become possible to perform realistic numerical simulations with high resolution, real topography, meteorological forcing, and lateral boundary conditions. These realistic simulations have (1) given us pictures of what the circulation looks like in the entire East Sea, which is insufficiently revealed by the observations, (2) expanded our understanding of the extent to which numerical configurations, such as small-scale parameterization, bottom topography, and horizontal/vertical resolution, affect a model's ability to represent the East Sea circulation, (3) provided a tool to study dynamical processes in the East Sea circulation. As ocean observational data have increased abundantly with advancing observing technologies such as Argo floats, satellites, and so on, ocean data assimilation techniques have been applied to numerical models in the East Sea. The approximate Kalman Filter and 3 D-Var methods have been applied to circulation models of the East Sea, resulting in operational forecast systems for the East Sea.

Despite extensive efforts of direct current measurements by current meter moorings and tracked floats since the 1990s, as well as studies based on hydrographic properties and numerical modeling, the thermohaline circulation and associated subsurface circulation of the East Sea remains somewhat elusive.

Especially, following issues have been identified as important processes that need to be addressed through more observational efforts and analytical/numerical modeling.

- An overarching question is whether or not the East Sea MOC is slowing down, while studies using chemical tracers have reported a decline in the formation of deep waters (Gamo 1999; Jenkins 2008). This may be answered by combining numerical modeling and long-term choke-point monitoring of currents.
- The driving mechanism of the deep-layer circulation is one of the least known problems. Presently, deep-water formation seems to be a more probable candidate than surface wind. Overall, there are still a number of issues to be resolved in order to understand well the circulation dynamics of the East Sea.
- Cyclonic penetration of deep waters from the JB to the UB and YB is a major conduit for oceanic climate signals to travel southward to the UB and YB from their origin in the JB. The climate signals would appear in the JB first, so it is important to examine the variability of this circulation. It is unclear what causes the observed inter-basin difference of seasonal and intraseasonal variation of deep currents. Interannual and longer term variations have not been adequately documented.
- It is an open question why the deep circulation of the UB is weakest among three deep basins, while mesoscale eddy activities in the UB are vigorous.
- Also required is an improved understanding of the coupling of upper and deep circulations, and of the role of surface processes such as air-sea flux and mesoscale eddies on the deep circulation.

Acknowledgements DK Lee was supported by Basic Science Research Program through the National Research Foundation of Korea (NRF) funded by the Ministry of Education (NRF-2014R1A1A2054910). YB Kim was supported by KIOST project (PE99292). YH Kim was supported by KIOST project (PE99295). CW Shin was supported by KIOST project (PE98921). KI Chang was supported by Ministry of Oceans and Fisheries of Korea through EAST-I project.

References

An HS (1974) On the cold water mass around the southeast coast of Korean Peninsula. J Oceanol Soc Korea 9:10–18

Arruda WZ, Nof D, O'Brien JJ (2004) Does the Ulleung eddy owe its existence to β and nonlinearity? Deep-Sea Res Part I 51:2073–2090

Baek GN, Seo S, Lee JH et al (2014) Characteristics of the flow in the Usan Trough in the East Sea. J Korean Soc Oceanogr 19:99–108 (in Korean)

Balmaseda MA, Smith GC, Haines K et al (2007) Historical reconstruction of the Atlantic Meridional Overturning Circulation from the ECMWF operational ocean reanalysis. Geophys Res Lett 34:L23615. doi:10.1029/2007GL031645

Bleck R, Smith LT (1990) A wind-driven isopycnic coordinate model of the north and equatorial Atlantic Ocean 1. Model development and supporting experiments. J Phys Oceanogr 95:3273–3285

Bleck R, Rooth C, Hu D et al (1992) Salinity-driven thermocline transients in a wind- and thermohaline-forced isopycnic coordinate model of the North Atlantic. J Phys Oceanogr 22:1486–1505

Byun SK (1989) Sea surface cold water near the southeastern coast of Korea: wind effect. J Oceanol Soc Korea 24:121–131
Byun SK, Seung YH (1984) Description of current structure and coastal upwelling in the southwest Japan Sea-summer 1981 and spring 1982. In: Ichiye T (ed) Ocean hydrodynamics of the Japan and East China Seas. Elsevier Oceanography Series 39, Amsterdam, pp 83–93
Byun SS, Park JJ, Chang KI, Schmitt RW (2010) Observation of near-inertial wave reflections within the thermostad layer of an anticyclonic mesoscale eddy. Geophys Res Lett 37:L01606. doi:10.1029/2009GL041601
Chang KI, Hogg NG, Suk MS et al (2002) Mean flow and variability in the southwestern East Sea. Deep-Sea Res Part I 49:2261–2279
Chang KI, Kim K, Kim YB et al (2009) Deep flow and transport through the Ulleung Interplain Gap in the southwestern East/Japan Sea. Deep-Sea Res Part I 56:61–72
Cho YK, Kim K (2000) Branching mechanism of the Tsushima Current in the Korea Strait. J Phys Oceanogr 30:2788–2797
Cho CB, Nam SH, Chang KI (2014) Subtidal temperature variability in stratified shelf water off the mid-east coast of Korea. Cont Shelf Res 75:41–53
Choi YJ, Yoon JH (2010) Structure and seasonal variability of the deep mean circulation of the East Sea (Sea of Japan). J Oceanogr 66:349–361
Clayson CA, Luneva M, Cunningham P (2008) Downwelling and upwelling regimes: connections between surface fronts and abyssal circulation. Dyn Atmos Ocean 45:165–186
Cox MD (1984) A primitive equation, three-dimensional model of the ocean. Ocean Group, GFDL, Princeton, NJ, Technical Report No 1
Csanady GT (1982) On the structure of transient upwelling events. J Phys Oceanogr 12:397–419
Falkowski PG, Ziemann D, Kolber Z et al (1991) Role of eddy pumping in enhancing primary production in the ocean. Nature 353:55–58
Fukamachi Y, Tanaka I, Ohshima KI et al (2008) Volume transport of the Soya Warm Current revealed by bottom-mounted ADCP and ocean-radar measurement. J Oceanogr 46:85–392
Fukudome K, Yoon JH, Ostrovskii A et al (2010) Seasonal volume transport variation in the Tsushima Warm Current through the Tsushima Straits from 10 years of ADCP observations. J Oceanogr 66:539–551
Fukumori I, Malanotte-Rizzoli P (1995) An approximate Kalman filter for ocean data assimilation: an example with an idealized Gulf Stream model. J Geophys Res 100:6777–6793
Gamo T (1999) Global warming may have slowed down the deep conveyor belt of a marginal sea of the northwestern Pacific: Japan Sea. Geophys Res Lett 26:3137–3140
Gamo T, Momoshima N, Tolmachyov S (2001) Recent upward shift of deep convection system in the Japan Sea, as inferred from the geochemical tracers tritium, oxygen, and nutrients. Geophys Res Lett 28:4143–4146
Godfrey JS (1989) A Sverdrup model of the depth-integrated flow for the world ocean allowing for island circulations. Geophys Astrophys Fluid Dyn 45:89–112
Gordon A, Giulivi C, Lee C et al (2002) Japan/East Sea intrathermocline eddies. J Phys Oceanogr 32:1960–1974
Haidvogel D, Beckmann A (1999) Numerical ocean circulation modeling. Imperial College Press, Singapore
Han MS, Jang DH, Yang HS (1998) The ecosystem of the southern coastal waters of the East Sea, Korea. II. Promary productivity in and around cold water mass. J Korean Soc Oceanogr 33:196–204
Hirose N, Kim CH, Yoon JH (1996) Heat budget in the Japan Sea. J Oceanogr 55:217–235
Hirose N, Fukumori I, Yoon JH (1999) Assimilation of TOPEX/Poseidon altimeter data with a reduced gravity model of the Japan Sea. J Oceanogr 55:53–64
Hirose N, Kawamura H, Lee HJ et al (2007) Sequential forecasting of the surface and subsurface conditions in the Japan Sea. J Oceanogr 63:467–481
Hogan PJ, Hulbert HE (2000) Impact of upper ocean-topographical coupling and isopycnal outcropping in Japan/East Sea models with 1/8° to 1/64° resolution. J Phys Oceanogr 30:2535–2561

Hogan PJ, Hulbert HE (2005) Sensitivity of simulated circulation dynamics to the choice of surface wind forcing in the Japan/East Sea. Deep-Sea Res Part II 52:1464–1489
Hogan PJ, Hurlburt HE (2006) Why do intrathermocline eddies form in the Japan/East Sea? A modeling perspective. Oceanography 19:134–143
Holloway G, Sou T, Eby M (1995) Dynamics of circulation of the Japan Sea. J Mar Res 53:539–569
Hyun JH, Kim D, Shin CW et al (2009) Enhanced phytoplankton and bacterioplankton production coupled to coastal upwelling and an anticyclonic eddy in the Ulleung Basin, East Sea. Aquat Microb Ecol 54:45–54
Ichiye T, Takano K (1988) Mesoscale eddies in the Sea of Japan. La Mer 26:69–76
Isobe A, Isoda Y (1997) Circulation in the Japan Basin, the northern part of the Japan Sea. J Oceanogr 53:373–381
Isoda Y (1994) Warm eddy movements in the eastern Japan Sea. J Oceanogr 50:1–15
Jang JH (2011) Spatial and temporal structure of low-frequency currents off Uljin in the East Sea. Dissertation, Seoul National University
Jenkins WJ (2008) The biogeochemical consequences of changing ventilation in the Japan/East Sea. Mar Chem 108:137–147
Kang DJ, Park S, Kim YG et al (2003) A moving-boundary box model (MBBM) for oceans in change: An application to the East/Japan Sea. Geophys Res Lett 30:1299. doi:10.1029/2002GL016486
Kantha LH, Clayson CA (2000) Numerical models of oceans and oceanic processes. International Geophysics Series, vol 66. Academic Press, New York
Katoh O, Teshima K, Kubota K et al (1996) Downstream transition of the Tsushima Current west of Kyushu in summer. J Oceanogr 52:93–108
Kawabe M (1982) Branching of the Tsushima Current in the Japan Sea. Part II: Numerical experiment. J Oceanogr Soc Japan 38:183–192
Kawamura H, Yoon JH, Ito T (2007) Formation rates of water masses in the Japan Sea. J Oceanogr 63:243–253
Kim YJ (2007) A study on the Japan/East Sea oceanic circulation using an ultra-high resolution model. Dissertation, Kyushu University
Kim CH, Kim K (1983) Characteristics and origin of the cold water mass along the east coast of Korea. J Oceanol Soc Korea 18:73–83 (in Korean)
Kim KR, Kim K (1996) What is happening in the East Sea (Japan Sea)? Recent chemical observations during CREAMS 93-96. J Korean Soc Oceanogr 31:164–172
Kim YH, Min HS (2008) Seasonal and interannual variability of the North Korean Cold Current in the East Sea reanalysis data. Ocean Polar Res 30:21–31
Kim KJ, Seung YH (1999) Formation and movement of the ESIW as modeled by MICOM. J Oceanogr 55:369–382
Kim CH, Yoon JH (1996) Modeling of the wind-driven circulation in the Japan Sea using a reduced-gravity model. J Oceanogr 52:359–373
Kim CH, Yoon JH (1999) A numerical modeling of the upper and the intermediate layer circulation in the Eat Sea. J Oceanogr 55:327–345
Kim K, Kim KR, Min DH et al (2001) Warming and structural changes in the East (Japan) Sea: a clue to future changes in global oceans? Geophys Res Lett 28:3293–3296
Kim K, Kim KR, Kim YG et al (2004a) Water masses and decadal variability in the East Sea (Sea of Japan). Prog Oceanogr 61:157–174
Kim K, Lyu SJ, Kim YG et al (2004b) Monitoring volume transport through measurement of cable voltage across the Korea Strait. J Atmos Ocean Tech 21:671–682
Kim YB, Chang KI, Kim K et al (2009a) Vertical structure of low frequency currents in the southwestern East Sea (Sea of Japan). J Oceanogr 65:259–271
Kim YH, Chang KI, Park J et al (2009b) Comparison between a reanalyzed product by the 3-dimensional variational assimilation technique and observations in the Ulleung Basin of the East/Japan Sea. J Mar Syst 78:249–264
Kim YB, Chang KI, Park JH et al (2013) Variability of the Dokdo Abyssal Current observed in the Ulleung Interplain Gap of the East/Japan Sea. Acta Oceanol Sin 32:12–23

Kuhlbrodt T, Griesel A, Montoya M et al (2007) On the driving processes of the Atlantic meridional overturning circulation. Rev Geophys 45:1–32
Kwak JH, Lee SH, Park HJ et al (2013) Monthly measured primary and new productivities in the Ulleung Basin as a biological "hot spot" in the East/Japan Sea. Biogeosciences 10:4405–4417
Lee JC (1983) Variations of sea level and sea surface temperature associated with wind-induced upwelling in the southeast coast of Korea in summer. J Oceanol Soc Korea 18:149–160
Lee JC, Chang KI (2014) Variability of the coastal current off Uljin in summer 2006. Ocean Polar Res 36:165–177 (in Korean)
Lee T, Kim IN (2003) Chemical imprints of the upwelled waters off the coast of the southern East Sea of Korea. J Korean Soc Oceanogr 38:101–110
Lee JC, Na JY (1985) Structure of upwelling off the southeast coast of Korea. J Oceanol Soc Korea 20:6–19
Lee DK, Niiler PP (2005) The energetic surface circulation patterns of the Japan/East Sea. Deep-Sea Res Part II 52:1547–1563
Lee DK, Niiler PP (2010a) Surface circulation in the southwestern Japan/East Sea as observed from drifters and sea surface height. Deep-Sea Res Part I 57:1222–1232
Lee DK, Niiler PP (2010b) Eddies in the southwestern East/Japan Sea. Deep-Sea Res Part I 57:1233–1242
Lee HC, Yoon JH (1994) On the free surface OGCM. In: Proceeding of fall meeting of Japan Oceanographical Society
Lee DK, Kwon JI, Hahn SB (1998) The wind effect on the cold water formation near Gampo-Ulgi coast. J Korean Fish Soc 31:359–371 (in Korean)
Lee HJ, Yoon JH, Kawamura H et al (2003a) Comparison of RIAMOM and MOM in modeling the East Sea/Japan Sea circulation. Ocean Polar Res 25:287–302
Lee JC, Kim DH, Kim JC (2003b) Observations of coastal upwelling at Ulsan in summer 1997. J Korean Soc Oceanogr 38:122–134
Lee CR, Park C, Moon CH (2004) Appearance of cold water and distribution of zooplankton off Ulsan-Gampo area, eastern coastal area of Korea. J Korean Soc Oceanogr 9:51–63 (in Korean)
Lee CM, Thomas LN, Yoshikawa Y (2006) Intermediate water formation at the Japan/East Sea subpolar front. Oceanography 19:110–121
Lee HJ, Park JH, Wimbush M et al (2011) Tidal effects on intermediate waters: a case study in the East/Japan Sea. J Phys Oceanogr 41:234–240
Lie HJ, Byun SK, Bang IK et al (1995) Physical structure of eddies in the southwestern East Sea. J Korean Soc Oceanogr 30:170–183
Luneva M, Clayson CA (2006) Connections between surface fluxes and deep circulations in the Sea of Japan. Geophys Res Lett 33:L24602. doi:10.1029/2006GL027350
Luyten JR, Pedlosky J, Stommel H (1983) The ventilated thermocline. J Phys Oceanogr 13:292–309
Lyu SJ, Kim K, Perkins HT (2002) Atmospheric pressure-forced subinertial variations in the transport through the Korea Strait. Geophys Res Lett 29(9):1294. doi:10.1029/2001GL014366
Martin S, Kawase M (1998) The southern flux of sea ice in the Tatarskiy Strait, Japan Sea and the generation of the Liman Current. J Mar Res 51:141–155
McCarthy G, Frajka-Williams E, Johns WE et al (2012) Observed annual variability of the Atlantic meridional overturning circulation at 26.5°N. Geophys Res Lett 39:L19609. doi:10.1029/2012GL052933
Minato S, Kimura R (1980) Volume transport of the western boundary current penetrating into a marginal sea. J Oceanogr Soc Japan 36:185–195
Mitchell DA, Teague WJ, Wimbush M et al (2005a) The Dok Cold Eddy. J Phys Oceanogr 35:273–288
Mitchell DA, Watts DR, Wimbush M et al (2005b) Upper circulation patterns in the Ulleung Basin. Deep-Sea Res Part II 52:1617–1638

Morimoto A, Yanagi T, Kaneko A (2000) Eddy field in the Japan Sea derived from satellite altimetric data. J Oceanogr 56:449–462
MSA Reports (1995–2007) Report of marine pollution surveys. Hydrographic Department, Maritime Safety Agency, Japan (in Japanese)
Na JY, Seo JW, Han SK (1992) Monthly-mean sea surface winds over the adjacent seas of the Korean Peninsula. J Oceanol Soc Korea 27:1–10
Nishida Y, Kanomata I, Tanaka I et al (2003) Seasonal and interannual variations of the volume transport through the Tsugaru Strait. Umi no Kenkyu 12:487–499 (in Japanese)
Nof D (1993) The penetration of Kuroshio water into the Sea of Japan. J Phys Oceanogr 23:797–807
Nof D (2000) Why much of the Atlantic circulation enters the Caribbean Sea and very little of the Pacific circulation enters the Sea of Japan. Prog Oceanogr 45:39–67
Ohshima KI (1994) The flow system in the Japan Sea caused by a sea level difference through shallow straits. J Geophys Res 99:9925–9940
Onitsuka G, Yanagi T, Yoon JH (2007) A numerical study on nutrient sources in the surface layer of the Japan Sea using a coupled physical-ecosystem model. J Geophys Res 112:C05042. doi:10.1029/2006JC003981
Ou HW (2001) A model of buoyant throughflow: with application to branching of the Tsushima Current. J Phys Oceanogr 31:115–126
Pacanowski RC, Dixon K, Rosati A (1991) The GFDL modular ocean model user guide. Geophysical Dynamics Laboratory, Princeton, USA, The GFDL Ocean Group, Technical Report No 2
Park YG (2007) The effects of Tsushima Warm Current on the interdecadal variability of the East/Japan Sea thermohaline circulation. Geophys Res Lett 34:L06609. doi:10.1029/2006GL029210
Park KA, Kim KR (2010) Unprecedented coastal upwelling in the East/Japan Sea and linkage to long-term large-scale variations. Geophys Res Lett 37:L09603. doi:10.1029/2009GL042231
Park JJ, Kim K (2013) Deep currents obtained from ARGO float trajectories in the Japan/East Sea. Deep-Sea Res Part II 85:169–181
Park JH, Watts DR (2005) Near-inertial oscillations interacting with mesoscale circulation in the southwestern Japan/East Sea. Geophys Res Lett 32:L10611. doi:10.1029/2005GL022936
Park YG, Oh KH, Chang KI et al (2004) Intermediate level circulation of the southwestern part of the East/Japan Sea estimated from autonomous isobaric profiling floats. Geophys Res Lett 31:L13213. doi:10.1029/2004GL020424
Park KA, Kim K, Cornillon PC et al (2006) Relationship between satellite-observed cold water along the Primorye coast and sea ice in the East Sea (the Sea of Japan). Geophys Res Lett 33:L10602. doi:10.1029/2005GL025611
Park YG, Choi A, Kim YH et al (2010) Direct flows from the Ulleung Basin into the Yamato Basin in the East/Japan Sea. Deep-Sea Res Part I 57:731–738
Park YG, Park JH, Lee HJ et al (2013) The effects of geothermal heating on the East/Japan Sea circulation. J Geophys Res 118:1893–1905. doi:10.1002/jgrc.20161
Postlethwaite CF, Rohling EJ, Jenkins WJ et al (2005) A tracer study of ventilation in the Japan/East Sea. Deep-Sea Res Part II 52:1684–1704
Rhines PB, Young WR (1982) A theory of the wind-driven circulation. J Mar Res 40:559–596
Senjyu T, Sudo H (1996) Interannual variation of the Upper Portion of the Japan Sea Proper Water and its probable cause. J Oceanogr 52:27–42
Senjyu T, Shin HR, Yoon JH et al (2005) Deep flow field in the Japan/East Sea as deduced from direct current measurements. Deep-Sea Res Part II 52:1726–1741
Seung YH (1974) A dynamic consideration on the temperature distribution in the east coast of Korea in August. J Oceanol Soc Korea 9(1–2):52–58 (in Korean)
Seung YH (1984) A numerical experiment of the effect of coastline geometry on the upwelling along the east coast of Korea. J Oceanol Soc Korea 19:24–30
Seung YH (1992) A simple model for separation of the East Korean Warm Current and formation of the North Korean Cold Current. J Oceanol Soc Korea 27:189–196

Seung YH (1997) Application of the ventilation theory to the East Sea. J Korean Soc Oceanogr 32:8–16
Seung YH (2003) Significance of shallow bottom friction in the dynamics of the Tsushima Current. J Oceanogr 59:113–118
Seung YH (2005a) Branching of the Tsushima Current by an abrupt increase of bottom depth. J Oceanogr 61:261–269
Seung YH (2005b) Abyssal currents driven by a local wind forcing through deep mixed layer: implication to the East Sea. Ocean Sci J 40:101–107
Seung YH (2012) Abyssal circulation driven by a periodic impulsive source in a small basin with steep bottom slope with implications to the East Sea. Ocean Polar Res 34:287–296
Seung YH, Kim K (1993) A numerical modeling of the East Sea circulation. J Oceanogr Soc Korea 28:292–304
Seung YH, Kim KJ (1997) Estimation of the residence time for renewal of the East Sea Intermediate Water using MICOM. J Korean Soc Oceanogr 32:17–27
Seung YH, Kim KJ (2011) Boundary currents in a meridional channel subject to seasonally varying buoyancy forcing: application to the Tsushima Current. J Oceanogr 67:563–575
Seung YH, Yoon JH (1995a) Some features of winter convection in the Japan Sea. J Oceanogr 51:61–73
Seung YH, Yoon JH (1995b) Robust diagnostic modeling of the Japan Sea circulation. J Oceanogr 51:421–440
Seung YH, Han SY, Lim EP (2012) Seasonal variation of volume transport through the straits of the East/Japan Sea viewed from the island rule. Ocean Polar Res 34:403–411
Shin HR, Byun SK, Kim C et al (1995) The characteristics of the structure of a warm eddy observed to the northwest of Ulleungdo in 1992. J Korean Soc Oceanogr 30:39–56 (in Korean)
Shin HR, Shin CW, Kim C et al (2005) Movement and structural variation of warm eddy WE92 for three years in the western East/Japan Sea. Deep-Sea Res Part II 52:1742–1762
Smith RL (1974) A description of current, wind and sea level variations during coastal upwelling off the Oregon coast. J Geophys Res 79:435–443
Son YT, Chang KI, Yoon ST et al (2014) A newly observed physical cause of the onset of the subsurface spring phytoplankton bloom in the southwestern East Sea/Sea of Japan. Biogeosciences 11:1–12
Spall MA (2002) Wind- and buoyancy-forced upper ocean circulation in two-strait marginal seas with application to the Japan/East Sea. J Geophys Res 107(C1). doi:10.1029/2001JC000966
Takematsu M, Nagano Z, Ostrovskii AG et al (1999a) Direct measurements of deep currents in the northern Japan Sea. J Oceanogr 55:207–216
Takematsu M, Ostrovskii AG, Nagano Z (1999b) Observations of eddies in the Japan Basin interior. J Oceanogr 55:237–246
Takikawa T, Yoon JH, Cho KD (2005) The Tsushima Warm Current through Tsushima Straits estimated from ferryboat ADCP data. J Phys Oceanogr 35:1154–1168
Talley L, Reid J, Robbins P (2003) Data-based meridional overturning streamfunctions for the global ocean. J Climate 16:3213–3224
Tanioka K (1968) On the East Korean Warm Current (Tosen Warm Current). Oceanogr Mag 20:31–38
Teague WJ, Jacobs GA, Hwang PA et al (2002) Low-frequency current observations in the Korea/Tsushima Strait. J Phys Oceanogr 32:621–1641
Teague WJ, Tracey KL, Watts DR et al (2005) Observed deep circulation in the Ulleung Basin. Deep-Sea Res Part II 52:1802–1826
Toba Y, Tomizawa K, Kurasawa Y et al (1982) Seasonal and year-to-year variability of the Tsushima-Tsugaru Warm Current system with its possible cause. La Mer 20:41–51
Tomosada A (1986) Generation and decay of Kuroshio warm-core rings. Deep-Sea Res 33:1475–1486
Tsujino H, Nakano H, Motoi T (2008) Mechanism of currents through the straits of the Japan Sea: Mean state and seasonal variation. J Oceanogr 64:141–161

Uda M (1934a) Oceanographic conditions of the Japan Sea and its adjacent waters. J Imp Fish Exp St 7:91–191 (in Japanese)
Uda M (1934b) The results of simultaneous oceanographical investigations in the Japan Sea and its adjacent waters in May and June, 1932. J Imp Fish Exp St 5:57–190 (in Japanese)
Weaver A, Courtier P (2001) Correlation modeling on the sphere using a generalizing diffusion equation. Q J Roy Meteor Soc 127:1815–1846
Yamada K, Ishizaka J, Nagata H (2005) Spatial and temporal variability of satellite estimated primary production in the Japan Sea from 1998 to 2002. J Oceanogr 61:857–869
Yang JY (1996) Current structure derived from satellite tracked drifter in the northern part of the East Sea. Dissertation, Seoul National University
Yang HS, Oh SJ, Lee HP et al (1998) Distribution of particulate organic matter in the Gampo upwelling area of the southwestern East Sea. J Korean Soc Oceanogr 33:157–167
Yang J, Lin X, Wu D (2013) Wind-driven exchanges between two basins: Some topographic and latitudinal effects. J Geophys Res 118:4585–4599. doi:10.1002/jgrc.20333
Yasuda I, Okuda K, Li J (1992) Evolution of a Kuroshio warm-core ring variability of the hydrographic structure. Deep-Sea Res 39(S1):S131–S161
Yoo S, Park J (2009) Why is the southwest the most productive region of the East Sea/Sea of Japan? J Mar Syst 78:301–315
Yoon JH (1982a) Numerical experiment on the circulation in the Japan Sea. Part I. Formation of the East Korean Warm Current. J Oceanogr Soc Japan 38:43–51
Yoon JH (1982b) Numerical experiment on the circulation in the Japan Sea. Part II. Influence of seasonal variations in atmospheric conditions on the Tsushima Current. J Oceanogr Soc Japan 38:81–94
Yoon JH, Kawamura H (2002) The formation and circulation of the Intermediate Water in the Japan Sea. J Oceanogr 58:197–211
Yoon JH, Abe K, Ogata T et al (2005) The effect of wind-stress curl on the Japan/East Sea circulation. Deep-Sea Res Part II 52:1827–1844
Yoshikawa Y (2012) An eddy-driven abyssal circulation in a bowl-shaped basin due to deep water formation. J Oceanogr 68:971–983
Yoshikawa Y, Awaji T, Akimoto K (1999) Formation and circulation processes of intermediate water in the Japan Sea. J Phys Oceanogr 29:1701–1722
Yoshikawa Y, Lee CM, Thomas LN (2012) The subpolar front of the Japan/East Sea. Part III: Competing roles of frontal dynamics and atmospheric forcing in driving ageostrophic vertical circulation and subduction. J Phys Oceangr 42:991–1011
You SH, Yoon JH (2004) Modelling of the Ryukyu Current along the Pacific side of the Ryukyu Islands. Pac Oceanogr 2:85–92
Zheng P, Wu D, Lin X et al (2010) Interannual variability of Kuroshio Current and its effect on the Nearshore Branch in Japan/East Sea. J Hydrodyn 22:305–311